NOAA Technical Memorandum ERL PMEL-31

OBSERVATIONS OF SOUTH ALASKAN COASTAL WINDS

R. M. Reynolds
S. A. Macklin
T. R. Hiester

Pacific Marine Environmental Laboratory
Seattle, Washington
July 1981

UNITED STATES DEPARTMENT OF COMMERCE
Malcolm Baldrige, Secretary

NATIONAL OCEANIC AND ATMOSPHERIC ADMINISTRATION
John V. Byrne, Administrator

Environmental Research Laboratories
George H. Ludwig Director

NOTICE

The Environmental Research Laboratories do not approve, recommend, nor endorse any proprietary product or proprietary material mentioned in this publication. No reference shall be made to the Environmental Research Laboratories or to this publication furnished by the Environmental Research Laboratories in any advertising or sales promotion which would indicate or imply that the Environmental Research Laboratories approve, recommend, or endorse any proprietary product or proprietary material mentioned herein, or which has as its purpose an intent to cause directly or indirectly the advertised product to be used or purchased because of this Environmental Research Laboratories publication.

CONTENTS

Figures

Tables

Observations of South Alaskan Coastal Winds

by

R. M. Reynolds, S. A. Macklin, and T. R. Hiester[1]

Pacific Marine Environmental Laboratory
Seattle, Washington 98105

[1]Batelle Laboratory
Richland, Washington 99352

ABSTRACT. Two main groups of offshore katabatic flow, fall winds and gravity winds, are defined and discussed. Climatological averages of the Alaskan synoptic weather network define those weather patterns that promote offshore flow on the south Alaskan coast.

Observations were taken over several years near the Malaspina Glacier on the south coast of Alaska using research ships, buoys, and on one occasion an instrumented aircraft. At the beach, winds blow offshore almost continuously in the winter, and at night in the summer. Their direction is seemingly unperturbed by synoptic variations. Within approximately 50 km of the beach, the wind is unpredictable by synoptic analysis. Upper-air soundings in this region reveal a complicated process whereby coastal air flows under the marine boundary layer and subsequently is absorbed into it by a process of entrainment and warming.

1. INTRODUCTION

This paper discusses offshore coastal winds and their transition to the oceanic regime. Land breezes are ubiquitous features of high-latitude mountainous coastlines, occurring on a variety of spatial and temporal scales. There is a dearth of observation concerning these flows and their transition, and indeed, some confusion as to their terminology.

We present in the sections to follow a general discussion of coastal wind types and the factors which serve to modify them offshore. An extensive set of observations which define the salient aspects of katabatic flows and their modification is presented and discussed.

1.1. Survey of Coastal Wind Types

Katabatic flow can be subdivided into two main groups, fall winds and gravity winds (Huschke, 1959). Both are driven by pressure force; the difference being one of scale.

Fall winds are large-scale phenomena, often driven by large-scale pressure gradients and requiring a reservoir of cold air from an elevated interior. The air is initially cold enough that it remains relatively cold

despite adiabatic warming during descent. A well-known example of a fall wind is the bora (from the Greek βνρεασ, meaning N-wind) which occurs on the Adriatic coast. Other locally named fall winds of some importance are the Mistral in southern France, the Athos in Greece, and the oroshi of Japan (Yoshino, 1975). As fall winds are driven by synoptic pressure patterns, they tend to appear suddenly, last for a few days, and then fade much more slowly than their onset. Temperatures drop by several degrees, and relative humidity often drops below 10% (ibid.). The outstanding characteristic of the bora is its gustiness and violent winds. As the cold air flows down to the sea, it accelerates and becomes highly turbulent (Defant, 1960).

Kilday (1970) has performed a study to determine the conditions favorable for the occurrence of bora winds in southeast Alaska (called Taku winds). It is possible to extend his arguments to other areas along the Gulf of Alaska coast. Fall winds occur where the terrain drops sharply and where there are mountain ranges near and parallel to the coast. If a very cold air mass passes over a mountain barrier, or if under the right pressure conditions, deeply chilled continental air is forced across the mountain ranges, the cold air cascades down the steep slopes to the warm coast. Observations indicate that the time of onset of wind is independent of a diurnal effect and maximum velocities can occur at any time of the day.

Fall winds can be classified as either cyclonic or anticyclonic depending on the overall synoptic pattern which might exist. In either case, isobars along the coast are tightly packed and winds blow predominantly across isobars and offshore (Fig. 1.1). The anticyclonic type produces strong, gusty winds with calm periods in between. The weather remains clear and dry. The cyclonic type is characterized by cloudy skies, snow, and only moderately cold temperatures. The same classifications and features are observed in the bora and mistral (Yoshino, 1975, p. 361).

Often large land/sea temperature differences are sufficient to produce near-continuous offshore flow. A cold continental air mass biases the interior pressure higher than the warmer ocean regions, equivalent to an anticyclonic fall wind. Often, these winds drain large river valleys such as the Susitna in southern Alaska. In this case, the drainage winds are channeled down Cook Inlet and dominate the winter wind field as far south as Augustine Island (Macklin et al., 1980). When that bias is accentuated by an approaching oceanic cyclone, the drainage winds can become quite intense.

The gravity wind is a much more local katabatic flow. Often called drainage wind, mountain wind, or katabatic wind interchangeably, it is caused by greater air density near the slope than that of the same level away from the slope. Highly dependent on net radiation at the surface, the air flows downhill in balance with frictional drag, the Earth's coriolis force, and the impressed synoptic scale pressure field. Because of rotation, the flow is inclined away from the line of steepest descent (Ball, 1960), but is still focused into valleys and estuaries where violent winds can occur. A particular type of drainage wind is the glacier wind, a continuous downdraft along the surface of the glacier which is relatively independent of insolation (Defant, 1960). Its thermal gradient is due to the temperature difference between the ice surface and the free air at the same altitude. In general, these winds are relatively light, but there are dramatic exceptions.

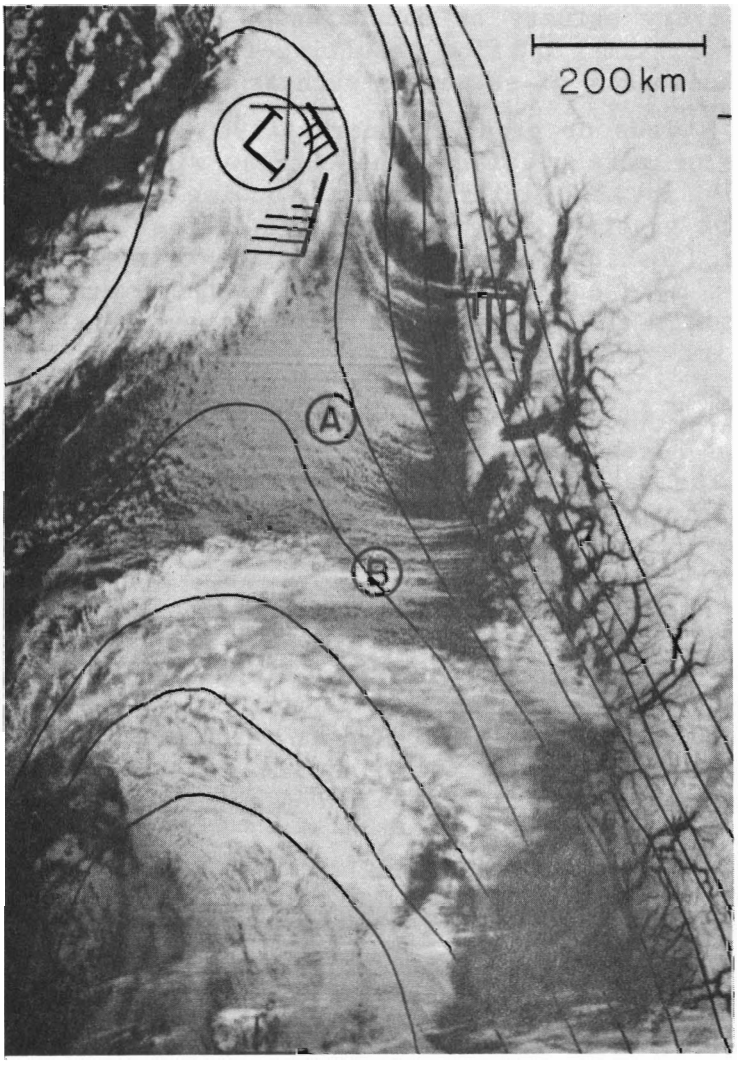

Figure 1.1. Satellite photograph of the Gulf of Alaska showing offshore winds and modification into the synoptic scale pattern.

A mountain wind is an even more localized katabatic flow which occurs on mountain sides, blowing down the flanks of the valleys and then down the valley axis (Defant, 1960; Yoshino, 1975).

Virtually every estuary on mountainous, high-latitude coastlines will be dominated by an axial outflow resulting from katabatic drainage. Often the winds at the mouths of estuaries such as Icy Bay on the coast of Alaska exhibit 50 ms^{-1} winds or greater (Searby, 1969). When the estuary is the terminus of one or more glaciers, the outflow winds are relatively persistent, especially in the winter months, showing little diurnal variation. Estuaries without glaciers exhibit much more diurnal katabatic winds, called nocturnal winds (Yoshino, 1975, p. 408). The cold air masses gathered on the upper slopes make up the first motion of the overall flow; they become the mountain wind in the valleys; and finally they are called land breeze on the coastal plain.

At the coast, an offshore wind often flows under the prevailing marine boundary layer. In the case of an existing land/sea breeze circulation it will underflow the larger circulation. A land breeze will be strengthened in this way (Yoshino, 1975, p. 160).

1.2 Offshore Modification of Coastal Winds

The offshore winds which have been discussed do not persist very far out to sea. The bora is seldom seen beyond 60 km (ibid., p. 366). Similarly, the Taku winds of southeast Alaska quickly merge into the open-ocean wind field. Figure 1.1 indicates a typical distance of 70 km for cross-isobaric fall winds to turn into a balanced open-ocean direction.

Surface friction alone cannot bring the winds into offshore balance in anything near the observed distances. Mahrt (1974) modeled the response of a layer-averaged neutral boundary layer flow to specified, time-dependent, pressure gradients, and found a frictional damping time (e^{-1} time scale) given by

$$T = h\{C_D[V]\cos\eta + w_E\}^{1}, \qquad (1.1)$$

where h is the layer height, C_D the drag coefficient, [V] a scale velocity (necessary for a linearized drag formulation), η is the angle between the layer-mean wind vector and the surface stress vector, and w_E is the entertainment rate. Typically, over the ocean $C_D = 1.5 \times 10^{-3}$, $[V] = 5\ ms^{-1}$, h = 1 km, and both η and w_E are small. In this case, T = 1½ days; with an advection velocity of 5 ms^{-1}, this corresponds to an adjustment distance of over 600 km.

However, for fall winds and gravity winds, the situation is much different. In the case of fall winds, the inversion base is lower; typically $h \tilde{\sim} 200$ m, and $[V] = 20\ ms^{-1}$. Entrainment is greatly enhanced; the cold air over a warm ocean generates buoyant thermals, which penetrate the inversion base. Surface-layer turbulence and shear-induced turbulence at the inversion base both contribute to the entrainment rate. It is likely there-

fore to have $w_E \tilde{\sim} 0.1$ ms^{-1}, which leads to adjustment times of ½ hr which corresponds to 30 km.

Gravity flows are generally much shallower, but the velocity is less also. Additionally, there is pronounced growth in h offshore. Mahrt's formulation does not apply to rapidly growing mixed layers, but an heuristic argument, based on equation (1.1) can be advanced. In his dissertation Reynolds (1980) shows that as the boundary layer becomes shallower, w_E becomes a strong function of h^{-1}. Therefore, equation (1) suggests that adjustment becomes weakly dependent on h.

When the synoptic pressure pattern directs a continental air mass offshore, the process of boundary layer growth and warming occurs on a much larger scale. Generally called air modification, it provides an important mechanism for the poleward flux of heat in the global energy balance, especially in the 40-50° latitude zone. One of the early analytical models of the boundary layer growth was an integrated, mixed-layer model by Businger (1954; 1972).

2. MEASUREMENTS OF COASTAL WINDS IN ALASKA

The research for this report is based on a collection of observations of coastal winds along the coast of Alaska. The measurements given here have been taken by the authors since 1975 and continue at this time.

Most of the measurements presented here were made in the vicinity of the Malaspina Glacier, a broad semicircular glacier on the coastal side of the dramatic St. Elias Mountains (Figs. 2.1 and 2.2). A vast entanglement of glaciers and snowfields in these mountains provides a source area for fall winds. As the air descends toward the coast, it is focused into Icy Bay and Yakutat Bay where winds are often observed by fishermen and weather observers (Searby, 1969).

2.1 Instruments and Analysis

Initial observation sets were simply standard ships' meteorological measurements of temperature, humidity (wet-bulb temperature), wind speed and direction, and some gross observations of sea state and clouds. The accuracy of ships' measurements have been discussed by Ching (1974) and Godshall et al. (1976). Wet- and dry-bulb temperatures were measured hourly at bridge height, 18.2 m above the ocean surface. During intercomparisons with other vessels and buoys during the GARP Atlantic Tropical Experiment (GATE), bridge temperatures were found accurate to 0.7°C. Winds were measured at mast height, 36 m. During the same GATE intercomparisons, these were shown to be accurate to approximately 1 ms^{-1}. It is understood that the above intercomparisons were made under optimum conditions; during routine operations, with the ship underway, the results are much poorer. It must continually be borne in mind that a sequence of ship observations is not concurrent, and can be treated as such only with care. Diurnal and synoptic scale processes can seriously contaminate the observed data.

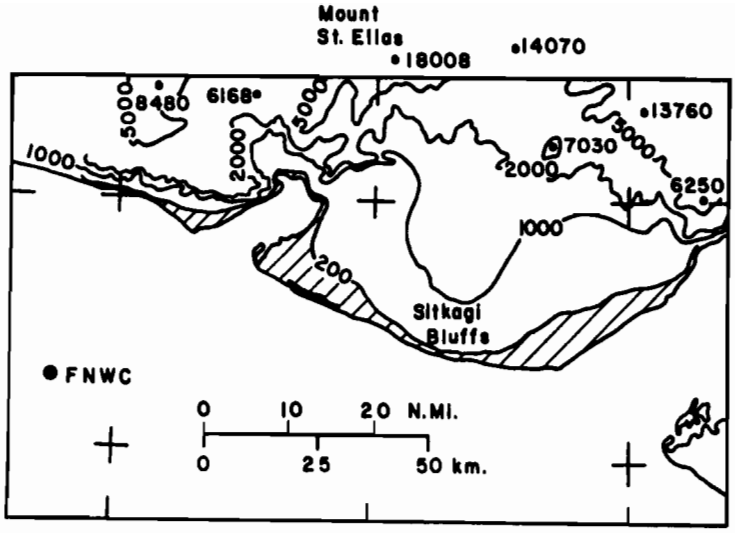

Figure 2.1 A Lambert conformal projection of the Malaspina Glacier showing elevations in feet. Shaded areas suggest the limit of the glacier.

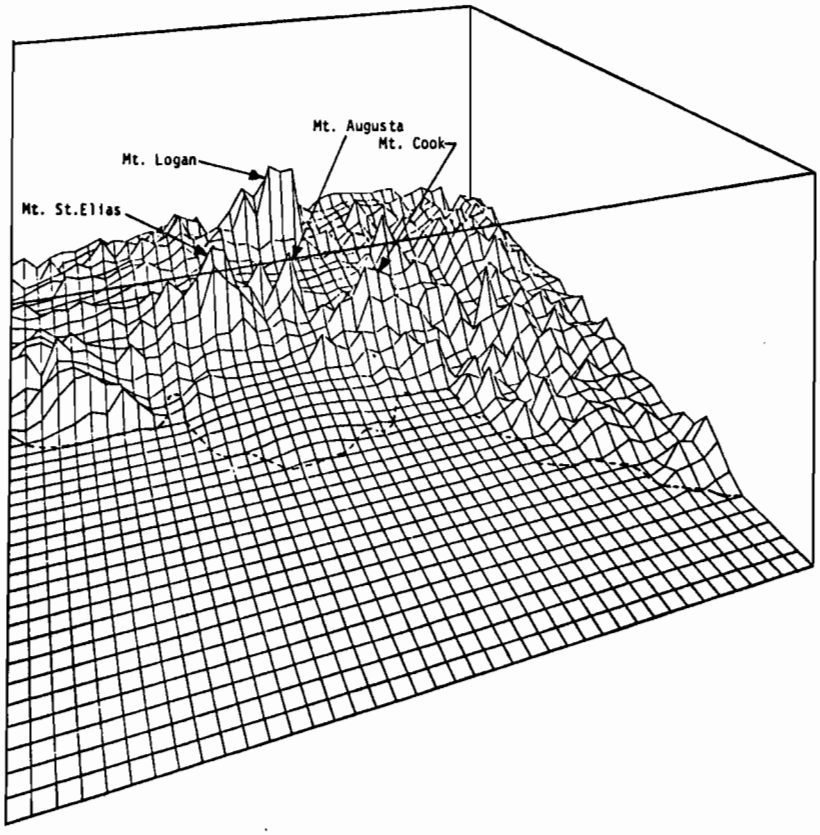

Figure 2.2 An isometric picture of the topography set on a 5-km grid.

From 1974 to 1977, during four cruises to the region, upper air data were collected with standard National Weather Service (NWS) radiosondes. The NWS radiosondes, older 403 MHz units, cycled between temperature, relative humidity, and reference channels in response to ambient pressure changes. Designed to profile the entire atmosphere, a pressure-actuated switching mechanism allowed only a few samples of the boundary layer, and the boundary layer and inversion base generally appeared as a confused decrease in temperature. Therefore, we needed to analyze our radiosonde charts to a much finer detail than is normally provided by NWS. We digitized as many points during a switch closure as possible in hopes of better resolving the lower profiles.

After 1977 a much more sophisticated 'airsonde' system provided greater detail of the lower troposphere. The airsonde makes over 50 samples through the boundary layer. A product of AIRCO, Inc., the sonde is a small winged styrofoam package weighing considerably less than the standard radiosonde. It has a pressure sensor and wet-/dry-bulb thermistors which are aspirated as the body spins on its tether during ascent. The themistors are accurate to 0.1°C, and the pressure sensor to 1 mb. These errors result in approximately 2% relative humidity uncertainty, or 2×10^4 in mixing ratio, and about 7 m height uncertainty. Neither of the above sounding systems has the capability of measuring winds aloft. Generally, conditions on the ship were unfavorable for performing the sensitive pibal measurements needed to deduce winds from the balloon trajectory.

On one occasion (see Fig. 2.20), a boundary layer profiler, supported by a kytoon, made detailed measurements of air temperature, wet-bulb temperature, wind speed, wind direction, and pressure. The pressure sensor malfunctioned, but reasonable height estimates were made in the following way: ascent and descent were scaled by matching heights at which sharp transitions in wind direction occurred and by assuming constant rates of ascent and descent; a radiosonde profile, taken just prior to kytoon launch, established an absolute height scale.

To ascertain the effects of the coastal mountain range on the offshore wind field, the authors analyzed data from several closely spaced meteorological stations (Fig. 2.3), including three National Data Buoy Office (NDBO) buoys. EB33 was placed at 58°30'N, 141°00'W, near the Malaspina Glacier. It had a boat-shaped (nomad style) hull (length = 6 m, beam = 3 m, depth = 2.5 m) and the sensors were approximately 5 m above the surface. From October 1974 to September 1976, it operated sporadically during the winters, but was reasonably reliable in the less stormy summers. The location of this buoy, about 150 km offshore, probably placed it beyond any near-coastal influences.

In the fall of 1976, the NDBO installed two buoys in the same vicinity, but much closer to shore. EB70 was deployed at 59°30'N, 140°12'W, approximately 60 km offshore. It was a 12 m discus hull buoy with all sensors located 10 m above the ocean surface. EB43 was a nomad hull similar to EB33, and was placed at 59°48'N, 142°00'W, only about 20 km offshore. These buoys operated from September 1976 to October 1977, but unfortunately, during the interesting months, November-January, EB43 was out of order.

The NDBO received all data by high frequency (HF) and satellite (GOES) transmissions. After editing the data they reduced it to standard archival

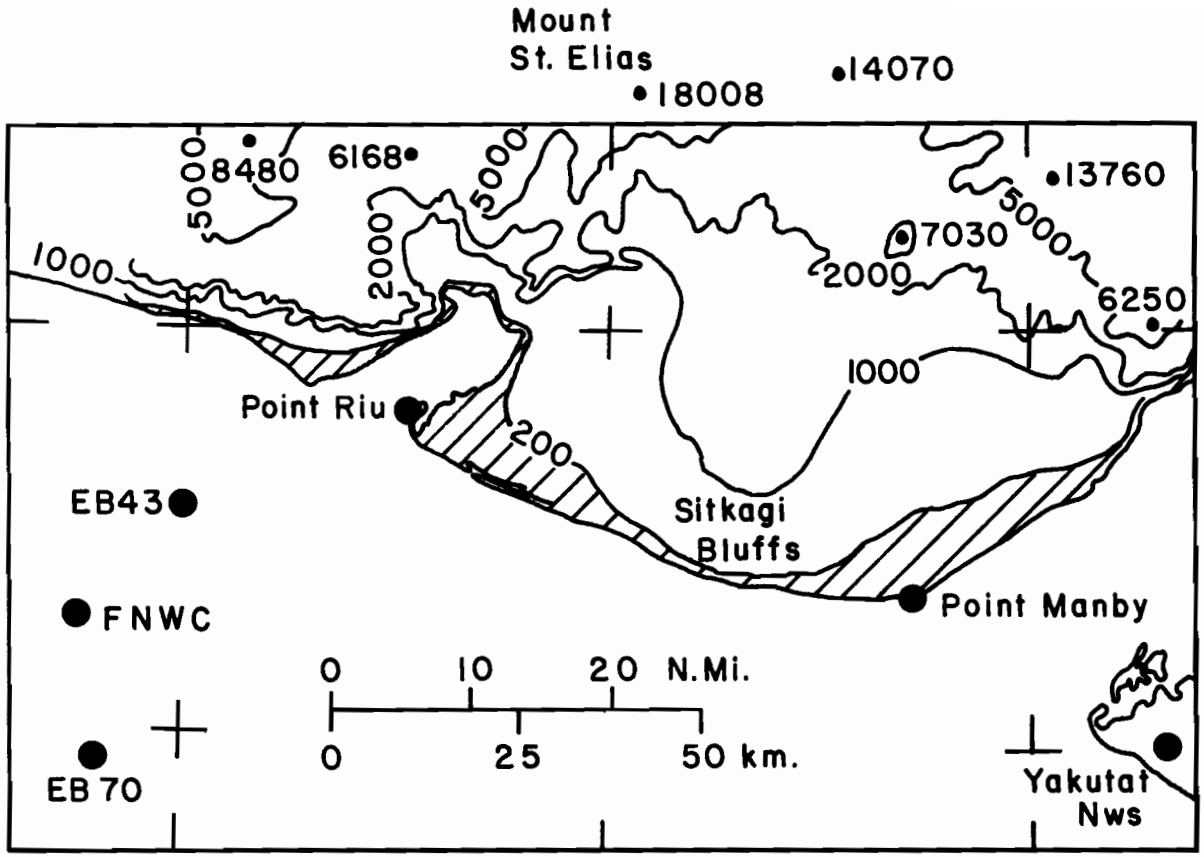

Figure 2.3. Same map as Figure 2.1. showing positions of meteorological stations used in this study.

format in which wind speed is given to the nearest mph and direction to the nearest 10°. The buoys averaged wind speed, direction, and air and sea temperatures over an 8-minute period and reported every 3 hours.

During the spring and summer of 1977, we measured coastal winds at two remote sites. Point Riou (59°55'N, 141°32'W) is at the mouth of Icy Bay and Point Manby (59°41'N, 140°17'W) is at the mouth of Yakutat Bay (Fig. 2.3). The stations, manufactured by Climatronics, Inc., recorded wind speed, wind direction, and air temperature on a 30-day strip chart with about the same accuracy as the data buoys.

At the Yakutat airport, a NWS facility provided hourly surface observations and twice-daily upper air soundings. The U.S. Navy's Fleet Numerical Weather Central (FNWC) provided surface winds from a synoptic scale pressure analysis. FNWC computes this analysis for their polar stereographic model, which has a mesh length of 481 km at 60°N. A geostrophic wind was determined (Bakun, 1973) by a computation of pressure gradient using a 5-point array centered at 59°39.9'N, 142°10.5'W (Fig. 2.3). They then approximated the surface wind by reducing the geostrophic wind by 30% and rotating it left by 15°.

Their analysis results from a blending of fields derived from past model runs, previous analysis extrapolated forward, and all current measurements of winds and pressure. The buoys are part of this set, and therefore FNWC-derived winds are not independent of them. However, after blending and smoothing the field on a synoptic scale we do not expect to see pronounced local effects in these winds.

From 21 February to 3 March, 1977, we flew tracklines off the Malaspina Glacier with an instrumented aircraft, the *Queen Air* (Fig. 2.4) (operated by the National Center for Atmospheric Research, (NCAR), Boulder, Colorado). Previous shipboard measurements were handicapped by the time necessary for a ship to move between stations. Temporal atmospheric processes interfered with the interpretation of the spatial atmospheric variations.

Possessing high quality instrumentation, a high-speed data logger, and a precision inertial navigational system (INS), the *Queen Air* could collect data sufficient to describe the turbulent behavior of the boundary layer (Lenschow, 1972). The three-dimensional wind field, temperature, humidity, and sea surface temperature are among the many measured parameters. At an airspeed of 250 km hr^{-1}, the *Queen Air* easily covered the Yakutat-Icy Bay area in 3½ hours. A typical flight plan is shown in Figure 2.5 and is summarized in Table 2.1.

Before undertaking any computations from flight data gathered during this period, we made a thorough appraisal of the quality of time series plots. All bad data could be avoided entirely by judiciously selecting continuous intervals of level flight and uniform heading from the time series for further processing. Because of drift in the aircraft's INS, the absolute wind speed is typically known only to within 2 ms^{-1} and wind direction to within 10°. Since the magnitude of these errors is time-dependent with a period of 84 minutes (Lenschow, 1972), relative differences between adjacent measurements are no more than 0.3 m/s over a 10 km averaging distance.

Figure 2.4. The research aircraft operated by the National Center for Atmospheric Research. The Queen Air is instrumented for low level turbulence measurements.

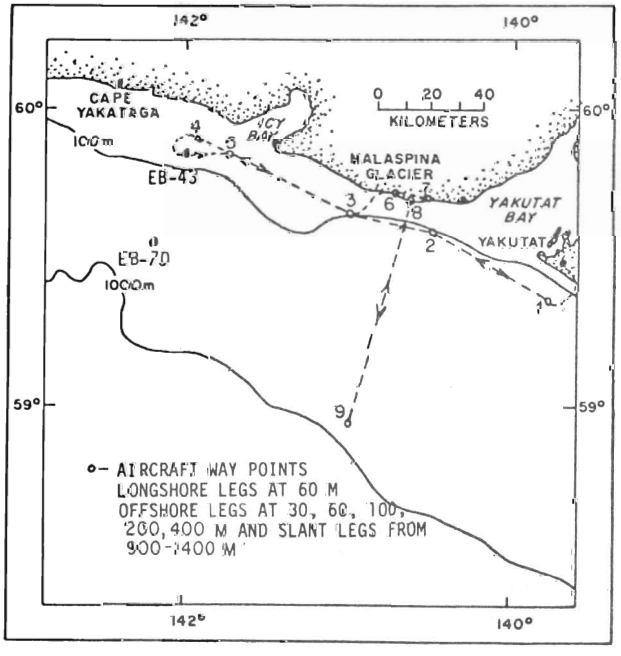

Figure 2.5. Typical flight plan for the Queen Air.

TABLE 2.1

Summary of Flight Plan for *Queen Air* off Yakutat Coastline

Way Points	Altitude (m)	Remarks
1,2,3	60	Longshore wind distribution.
6,7	15-180	Vertical sounding at coast, lower level.
7,6	180-900	Vertical sounding at coast, upper level.
8,9	30	Offshore wind distribution and vertical structure including upper air conditions.
9,8	100	
8,9	200	
9,8	400	
8,9	900-1350	
9,8	60	
3,4	60	Longshore variation.
4,5	60	Check INS with EB43 position comparison.
5,3,2,1	60	Return home, repeat measurements allow improved error analysis.

A standard time series analysis package, developed as a general tool, produced useful graphics for all the time series shown here. Aside from routine plots of speed, direction, temperature, etc., which need no explanation, a most useful graphic was the fabric diagram in various forms. The name fabric diagram is borrowed from a similar graphic developed by Davis and Ekern (1977). An example of the four forms of the plot is given in Figure 2.6.

A brief summary of the construction of the fabric diagram follows: A 41 x 41 grid of possible u,v wind vector components defines 40 x 40 boxes on a space where the polar radius is proportional to the square root of the wind speed, $r \propto \sqrt{s}$. All the data to be analyzed are sorted according to the wind vector, and the cumulative amount of a chosen quantity--number of occurrences, wind stress, heat flux, temperature variance--is calculated for each box of the grid. Finally, a 5 x 5 top-hat, smoothing kernel (not a box-car) is run over the grid to effect a reasonable picture. The grid is contoured with a simple linear interpolation routine. Contours represent 1% of the total accumulation per 1% area of the enclosed circle. Wind direction is plotted according to meteorological convention, the true compass direction from which the wind is blowing. By plotting wind speed as the square of the radius, equal areas of contours represent equal percentages, thus compensating for the spreading of radial line segments.

The frequency fabric diagram (Fig. 2.6) is basically a contour map of the wind velocity probability distribution. The probability of winds occurring in any velocity range are calculable from this diagram. The wind stress or energy fabric diagram is a contour of the % total energy (expressed as a square of the wind speed) per 1% area of the circle. While this plot is often similar to the frequency diagram, it occasionally points out highly preferred directions for the stress. As the ocean responds to wind stress and not frequency, this plot is valuable to the physical oceanographer.

Fabric diagrams are applied to the observed temperature in two ways. If surface temperature is available, then the heat flux fabric diagram is estimated by $H_o = U(\theta_{sfc} - \theta_{air})\ [C_D\rho]$ for each box. If θ_{sfc} is not available, then the average $\bar{\theta}_{air}$ over the record may be substituted for θ_{sfc}. Another useful variation is to calculate the temperature perturbation $\delta\theta = (\theta - \bar{\theta})$ for each box. The resulting temperature perturbation fabric diagram points out preferred winds which accompany warmer or colder air. Figure 2.6 points out a sharply defined range of wind speeds and directions which advect colder air to the site. This will be discussed in greater detail in Section 2.3. Finally, the temperature variance fabric diagram points out regions which contribute to the variance of the series.

2.2 Weather Patterns Over the South Alaskan Coast

The Gulf of Alaska is a region of extremely changeable sea-level pressure. Two winter features of the monthly mean barometric pressure field (Fig. 2.7) are the Aleutian Low, which dominates the North Pacific, and the Continental High which covers the main land masses of Siberia, Alaska, and British Columbia. In summer, increased heating over land produces a relatively low-pressure continental region which weakens the Aleutian Low; in

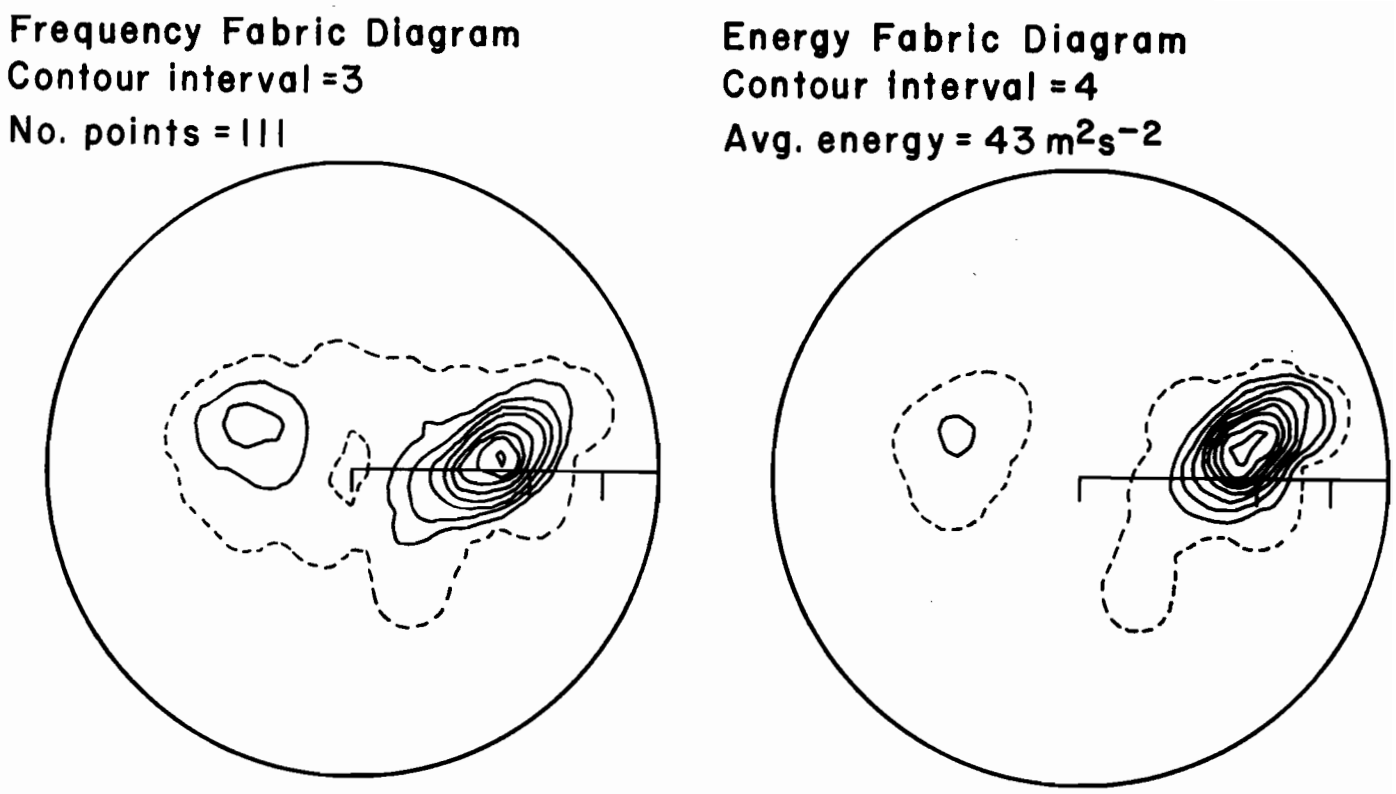

Figure 2.6(a). Typical fabric diagrams of wind frequency and energy. The data is from EB43 for the period of 6 March to 3 April, 1977.

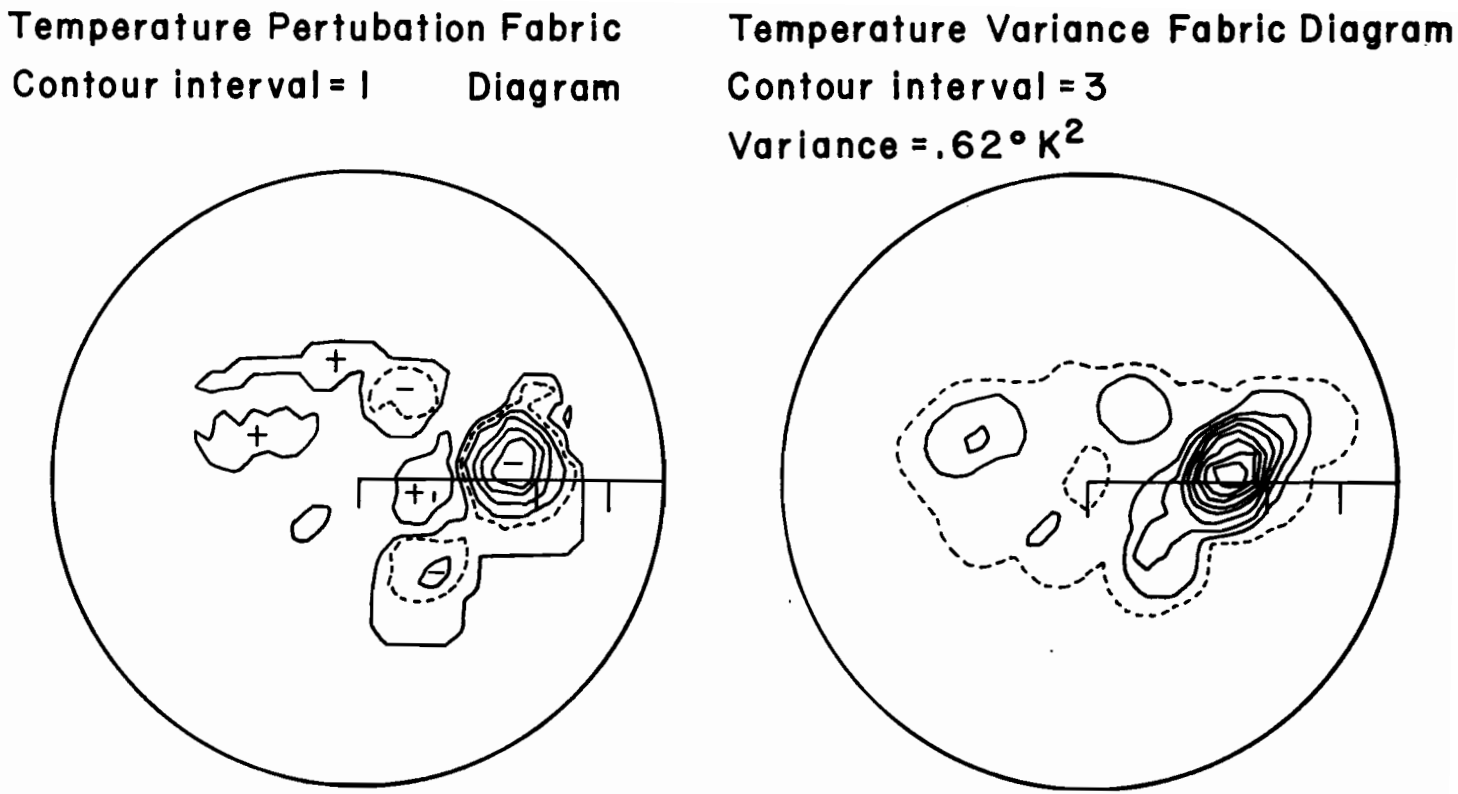

Figure 2.6(b). Fabric diagrams of temperature pertubation and variance for the same data as 2.6(a).

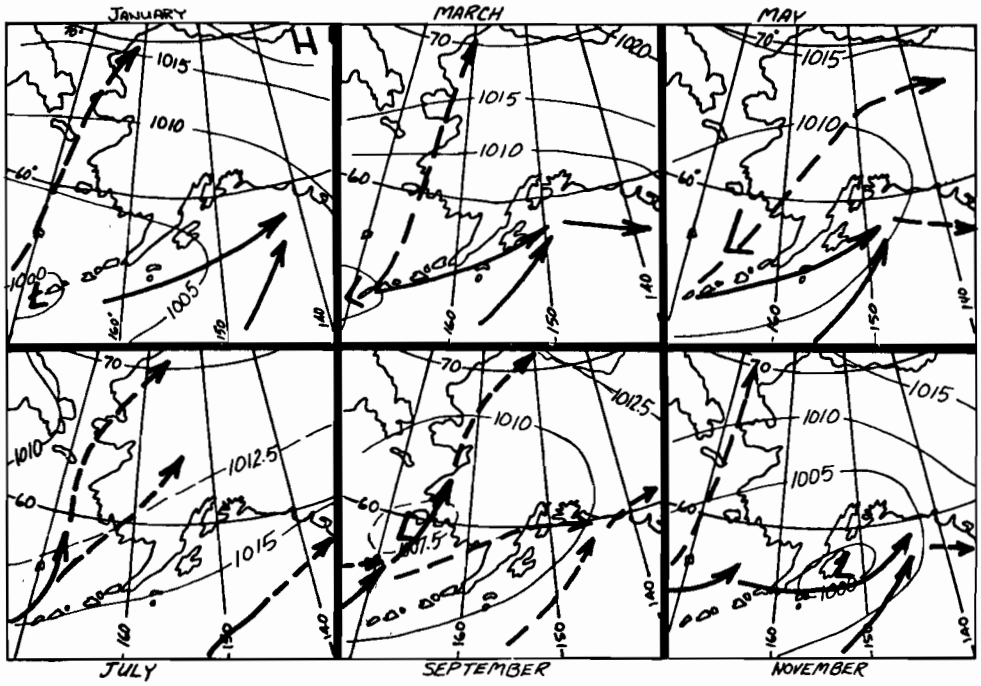

Figure 2.7. Average meteorological conditions in the Gulf of Alaska for various months of the year. Solid arrows are principal storm tracks, dashed arrows are secondary tracks. (From Searby, 1969)

winter excess terrestrial cooling produces the Continental High and amplifies the Aleutian Low. The trough of the Aleutian Low controls the passage of an endless stream of cyclonic disturbances traveling eastward across the North Pacific. Figure 2.7 shows average storm tracks for various times of the year wherein the effect of the Aleutian Low is evident.

Mean pressure fields bear little resemblance to the actual distribution at any time. In an attempt to treat statistically the daily weather patterns for the Alaskan region, Putnins (1966) analyzed over 18 years of surface and 500-mb weather maps. After developing a classification scheme which described 22 synoptic patterns, he determined the frequency of these patterns for each month of the year. Figures 2.8 (a-d) are a sample of his results, the six most common weather types for 4 months, representing each season. The figures are real maps selected as typical for the classification type. The nature of the main barometric features of the pressure field is apparent in these maps, especially the Aleutian Low. The convergence of cyclonic disturbances into the Gulf of Alaska is also apparent. Observed winds are reported with the following convention: indicators point in the direction from which the wind is blowing, one full barb represents a speed of 5 ms^{-1}, one-half barb indicates 2.4 ms^{-1}, and no barb implies wind speed less than 1.24 $ms^{-1}/2$.

The coastal mountains of British Columbia and Alaska present a barrier to the movement of disturbances with the result that many of them stagnate in the Gulf of Alaska for several days, especially if there is inland high pressure. Occasionally, if unable to move forward, these cyclones take a retrograde course toward the northwest. As Bilello noted in 1974, once a storm has moved against the mountain ranges bordering the northern Gulf of Alaska, only a vigorous circulation aloft can cause it to move further. With moderate southerly winds, maritime air moves into the coastal valleys and the front then has a tendency to become stationary along the Alaska Range. Strong southwesterly winds, however, occasionally force the front further up the valleys. At this point there is no definite physical barrier to impede movement of the front so it can now readily penetrate to the interior of the state and influence the weather accordingly. Nevertheless, exactly how far inland the front moves is dependent almost entirely upon the strength and persistence of the steering level winds. As marine air crosses the Alaska Range, a great deal of orographically induced precipitation occurs. For example, Middleton Island (150 km south of the coast) has 1.47 m of annual rainfall while there is a prodigious precipitation measured at coastal stations such as Cape St. Elias and Yakutat (3.36 m).

Based on the criterion for a fall wind condition as outlined in Section 1.1, patterns such a A, A_1, or D are appropriate to drive a fall wind from the high snow plateaus of the St. Elias Mountains. The frequency of occurrence of these patterns--marked in the upper right-hand corner of each pattern--varies from about 5% in the summer to 40% in the winter.

2.3 Observations at the Malaspina Glacier

During late 1974 and 1975, EB33 made wind measurements 150 km offshore of the Malaspina Glacier. When compared to winds computed from the global model of FNWC a slight preference for a bimodal wind field appears

(a) FEBRUARY

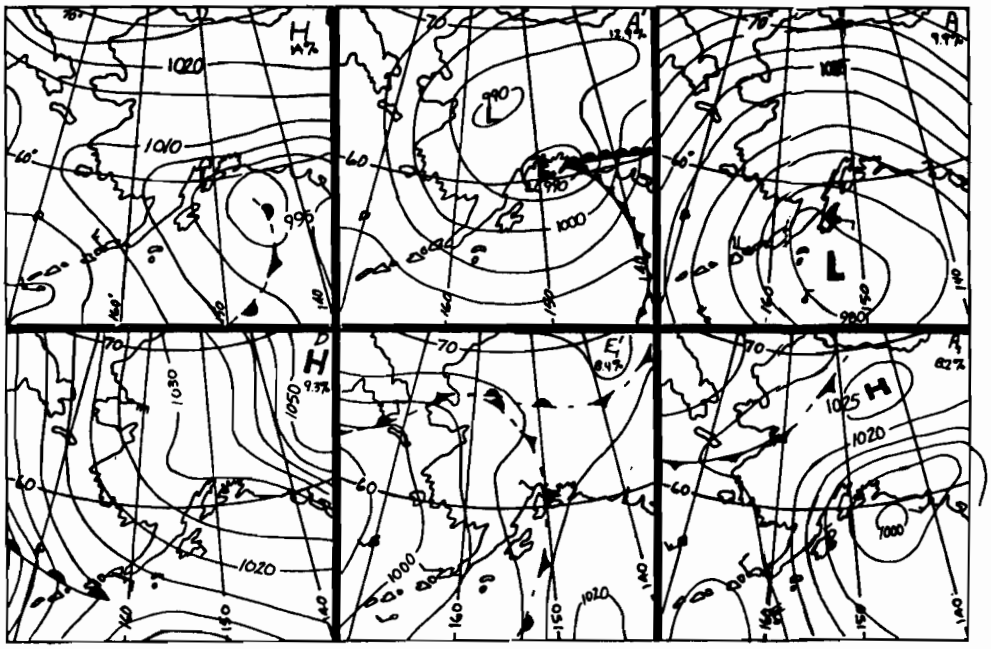

(b) NOVEMBER

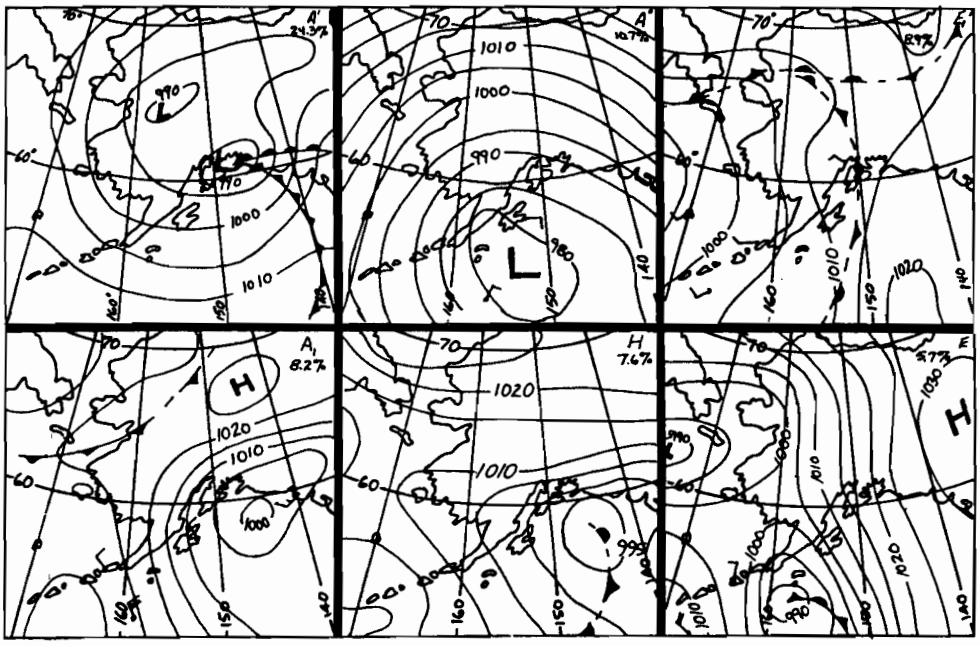

Figure 2.8(a)(b). Most common synoptic scale types as classified by Putnins (1966). Classification symbol and percentage of occurance are shown in the upper right hand corners.

(c) MAY

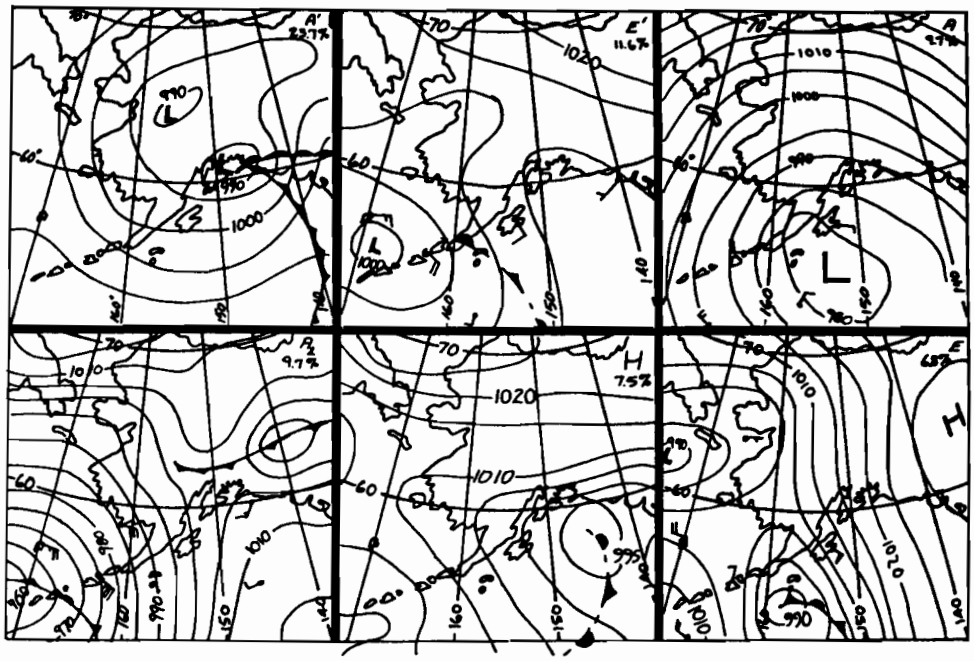

(d) AUGUST

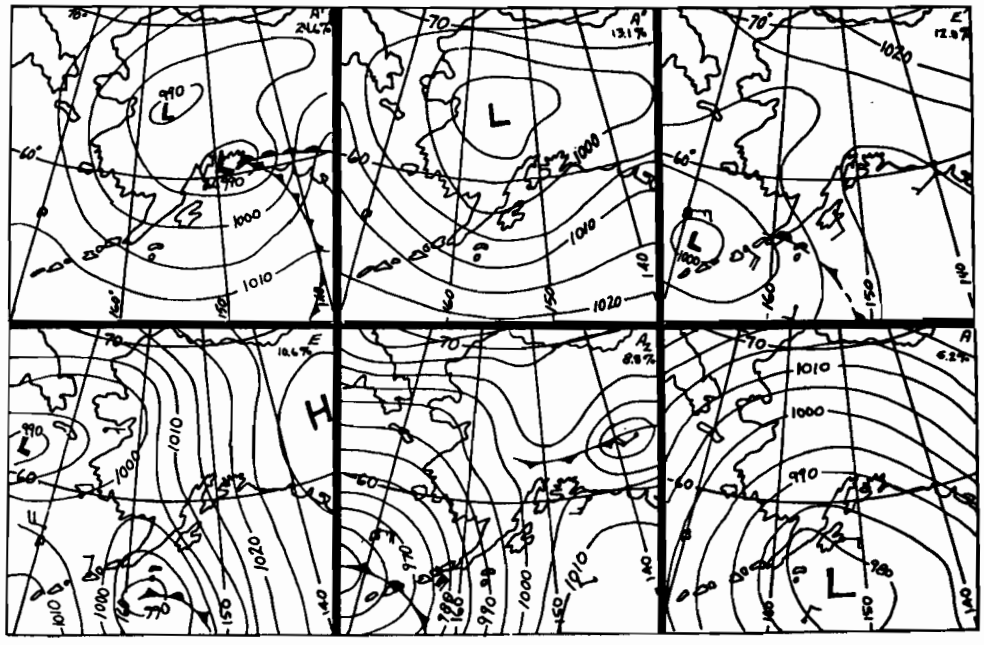

Figure 2.8(c)(d). Most common synoptic scale types as classified by Putnins (1966). Classification symbol and percentage of occurance are shown in the upper right corners.

(Fig. 2.9). In the winter of 1974/75 there were many occurrences of cold air outbreaks; the air would be up to 10° colder than the sea surface at this place for four days to a week duration. In spite of a fairly broad distribution of wind directions, the winds from the east, particularly the NE or ENE carried the coldest air (Fig. 2.10). It will be shown later that this is in keeping with the notion of large-scale air modification, where the isobars offshore are roughly perpendicular to the coastline. Such would be the case for pattern H or A_1 in Figure 2.8 if the low center were displaced to the east. That is, the continental air mass which falls offshore aligns with the isobars of a low-pressure disturbance and produces cold easterlies at the buoy (Fig. 2.11).

The NDBO installed buoys EB43 and EB70 in late 1976 and they operated sporadically throughout 1977. They were located much closer to shore than EB33 (10 and 60 km respectively), and hence we hoped to see a stronger coastal influence. The remote coastal stations at Point Riou and Point Manby operated reasonably well during their stay; they failed only as a result of occasional bear maulings. All stations operated well during two time periods: 6 March to 3 April and 6 June to 6 July.

The FNWC-derived surface winds for these time periods show a broad range of directions (Figs. 2.12, 2.13). Wind directions exhibited a counterclockwise rotation indicative of the passage of cyclonic disturbances to the south. The more frequent westerly winds in the May diagram result from a stagnant system which occurred during the first part of the period. Data from a single month are insufficient to assess whether such prolonged winds were typical.

Data buoys and land stations recorded wind events which appeared on the FNWC record. The land stations showed the events with a much reduced wind speed while the buoys showed only a slight reduction in wind speed from EB70 to EB43 (which was positioned closer to shore). The wind speed of FNWC inexplicably agrees more closely with EB43. Overall, wind speed correlation coefficients between the data buoys and FNWC are from 0.70 to 0.85.

Wind fabric diagrams (Figs 2.14, 2.15) show that winds at the four stations are different. The FNWC winds exhibit no special preference for direction while all the measured winds showed distinct influence of the coastline. EB70 had an almost symmetrical bimodal character with the most common wind directions approximately 115° and 270°. EB43 data showed bimodality also, but during March the winds from the east were more common (probably an offshore manifestation of the winter drainage winds from Malaspina Glacier). During summer, winds at EB43 were more common from the west, and the two buoys were better correlated. Coastal winds measured at Point Riou and Point Manby showed definite orographic influence. During winter at Point Riou, the combined katabatic drainage winds and mountain blockage resulted in winds that blew almost continuously from the northeast, down the glacier. In addition to orographic influence, diurnal forcing was apparent during both March and May. During the coldest period of the day, northerly drainage flow from the glacier dominated; in the daylight hours the flow was more often from the northeast and east.

We extracted additional details of the flow distribution by the use of correlation plots in which wind directions from two different records were plotted on the same graph. Points clustering about a 45° line represent

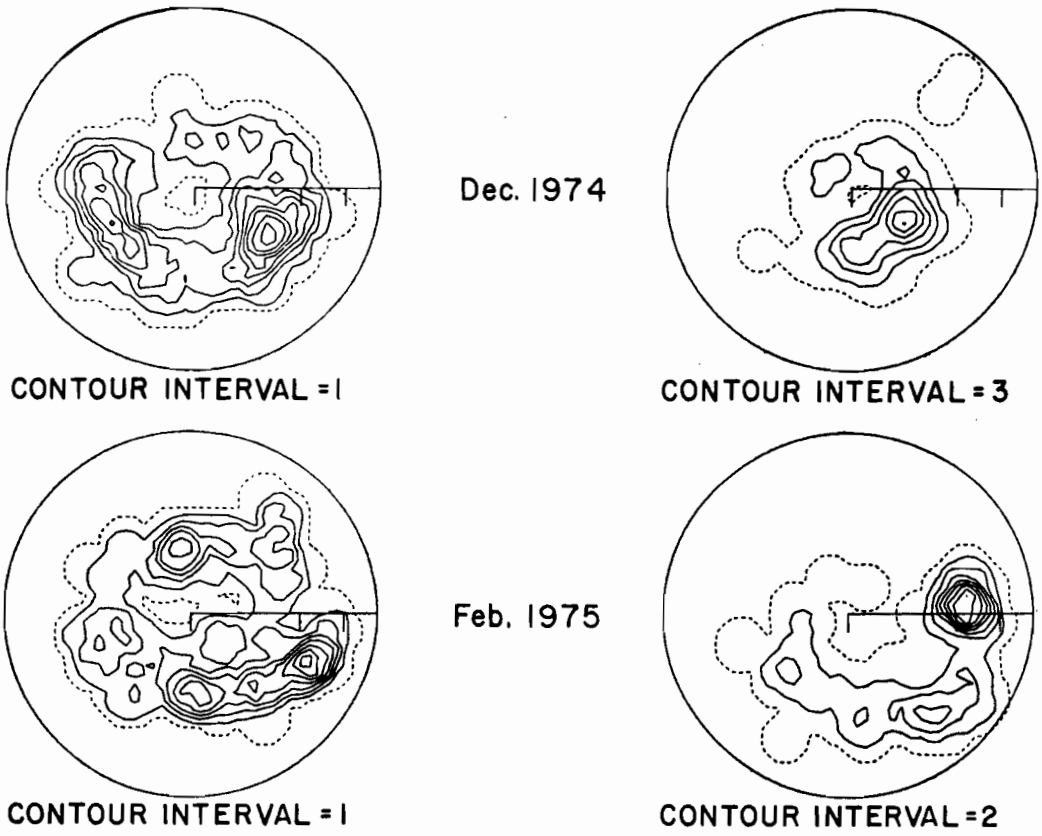

Figure 2.9(a). Fabric diagrams of wind observations at EB33 compared with those computed by FNWC. The circle represents a 30 ms^{-1} wind and ticks mark 10 and 20 ms^{-1} speed.

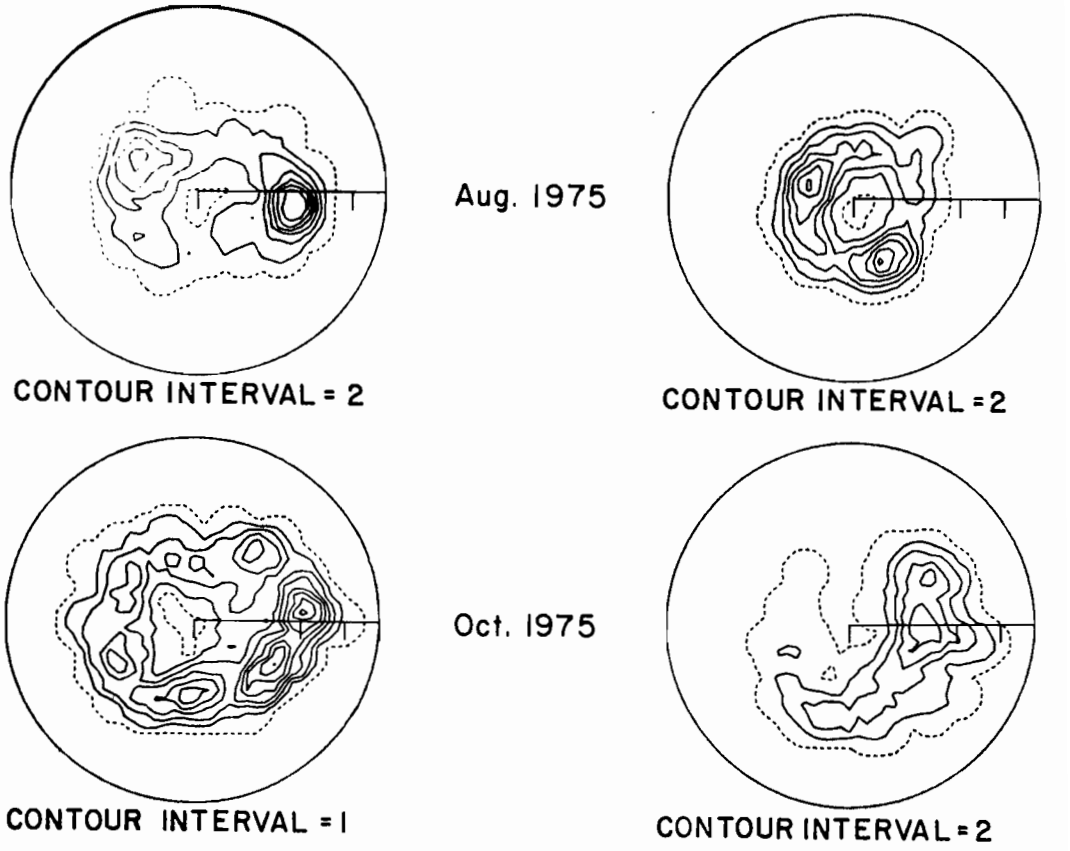

Figure 2.9(b). Fabric diagrams of wind observations at EB33 (left side) compared with those computed by FNWC.

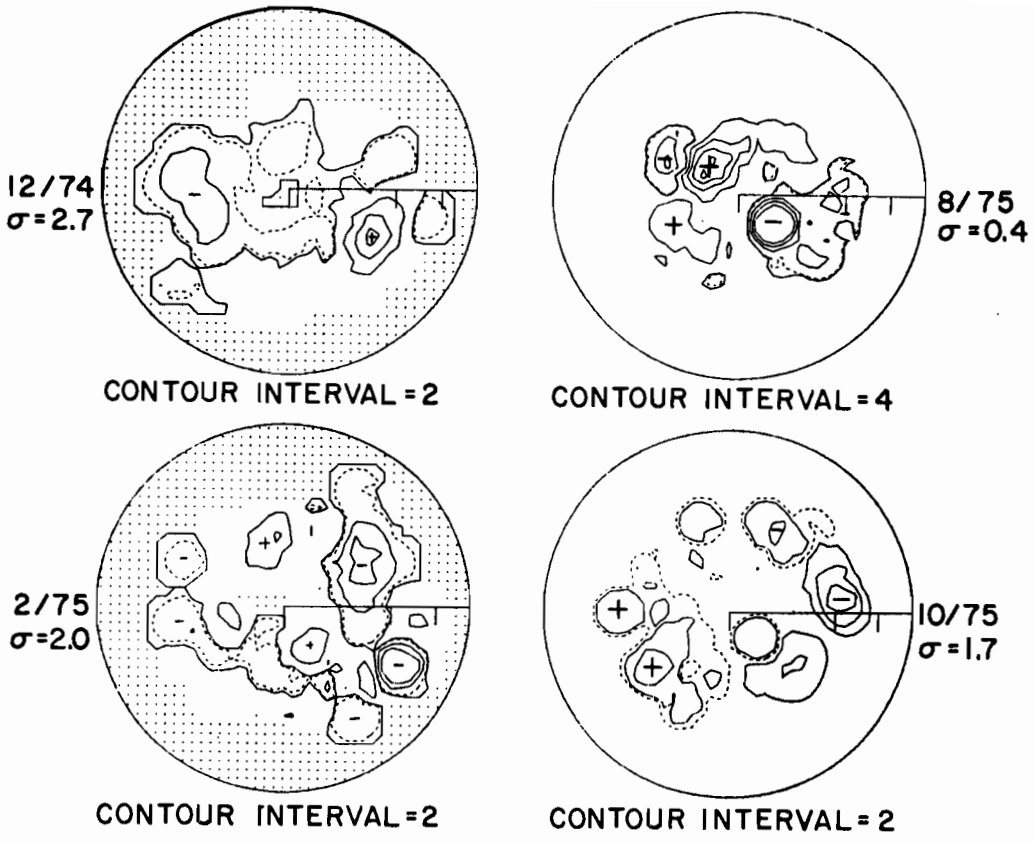

Figure 2.10. Temperature perturbation fabric diagrams for four months for EB33, 150 km offshore of Malaspina Glacier, AK. The variance of temperature is shown each month.

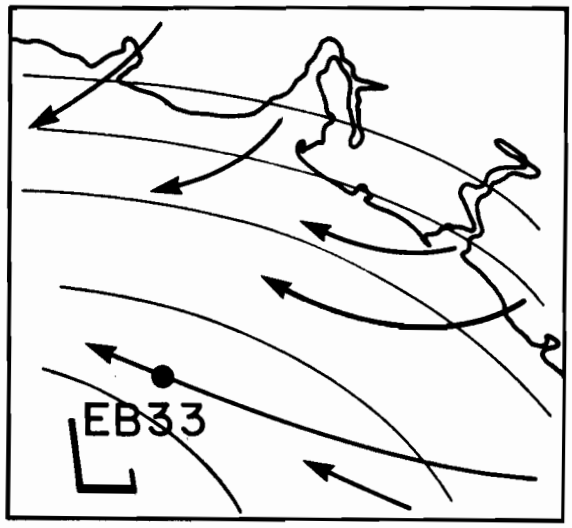

Figure 2.11. Schematic of a typical wind field on the Alaskan coast in which EB33 registers cold air.

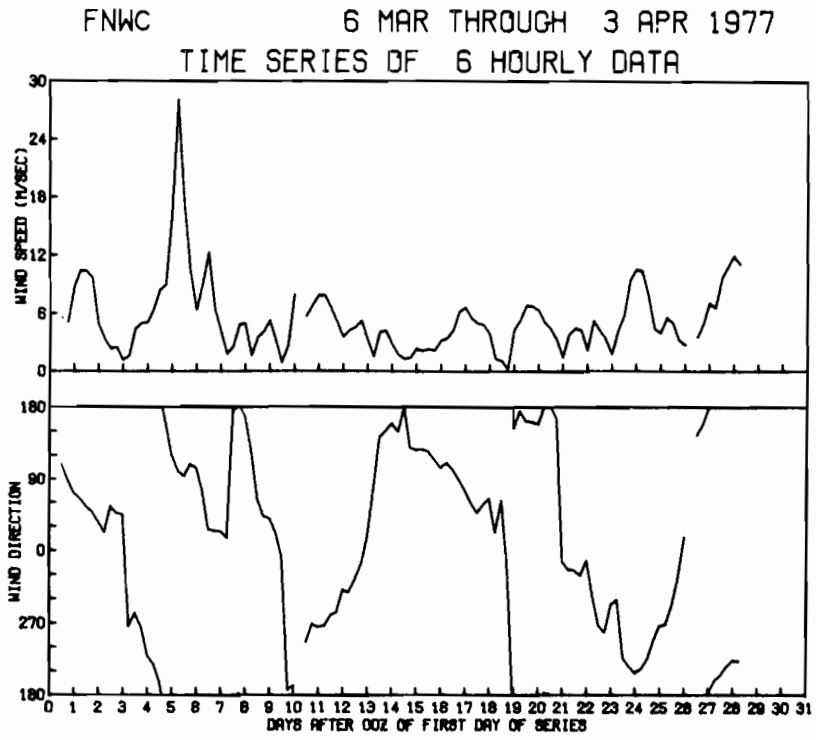

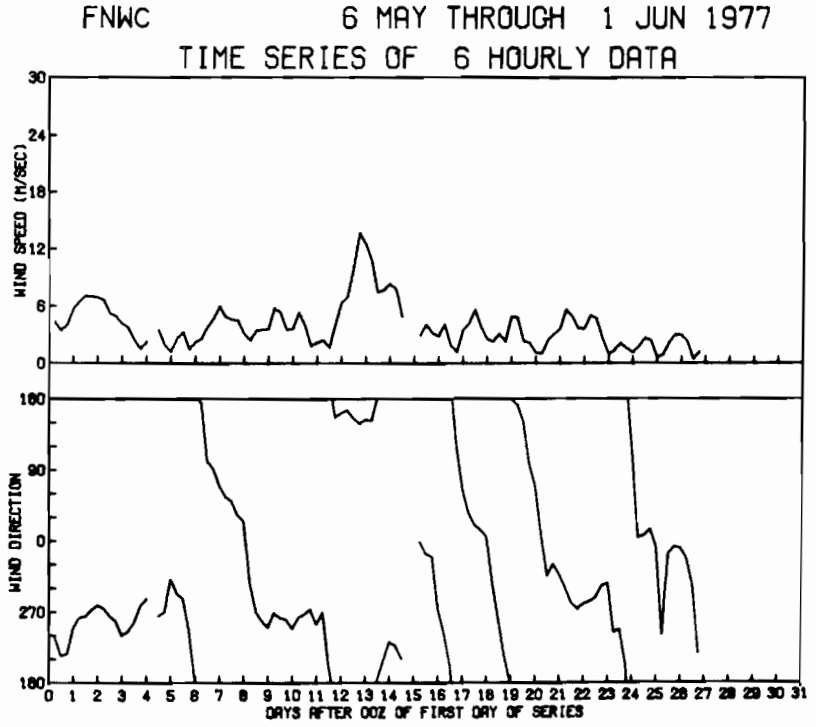

Figure 2.12. Time series of wind speed and direction as computed by FNWC for the two time periods of interest.

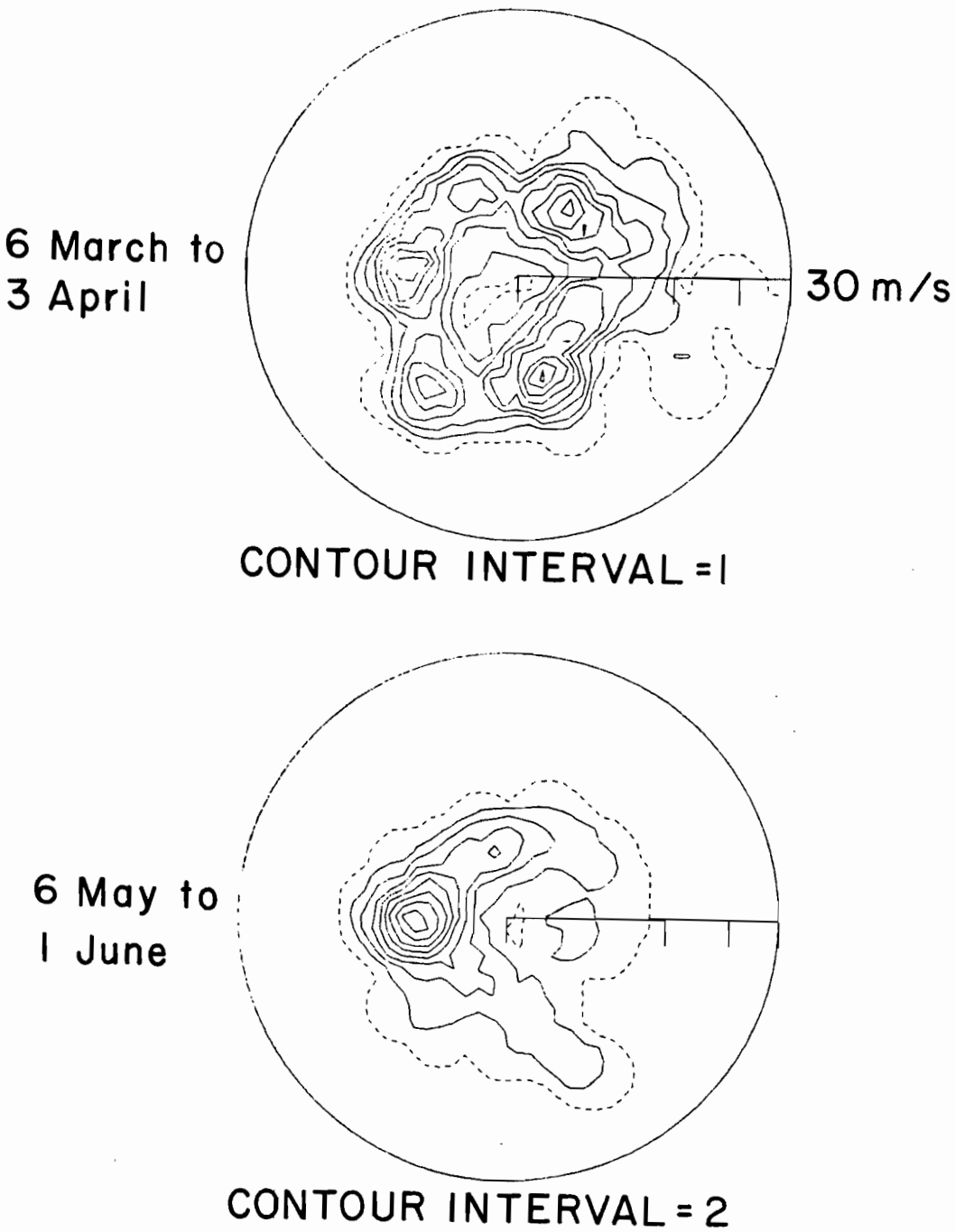

Figure 2.13. Fabric diagrams of winds computed by FNWC for the two time periods of interest.

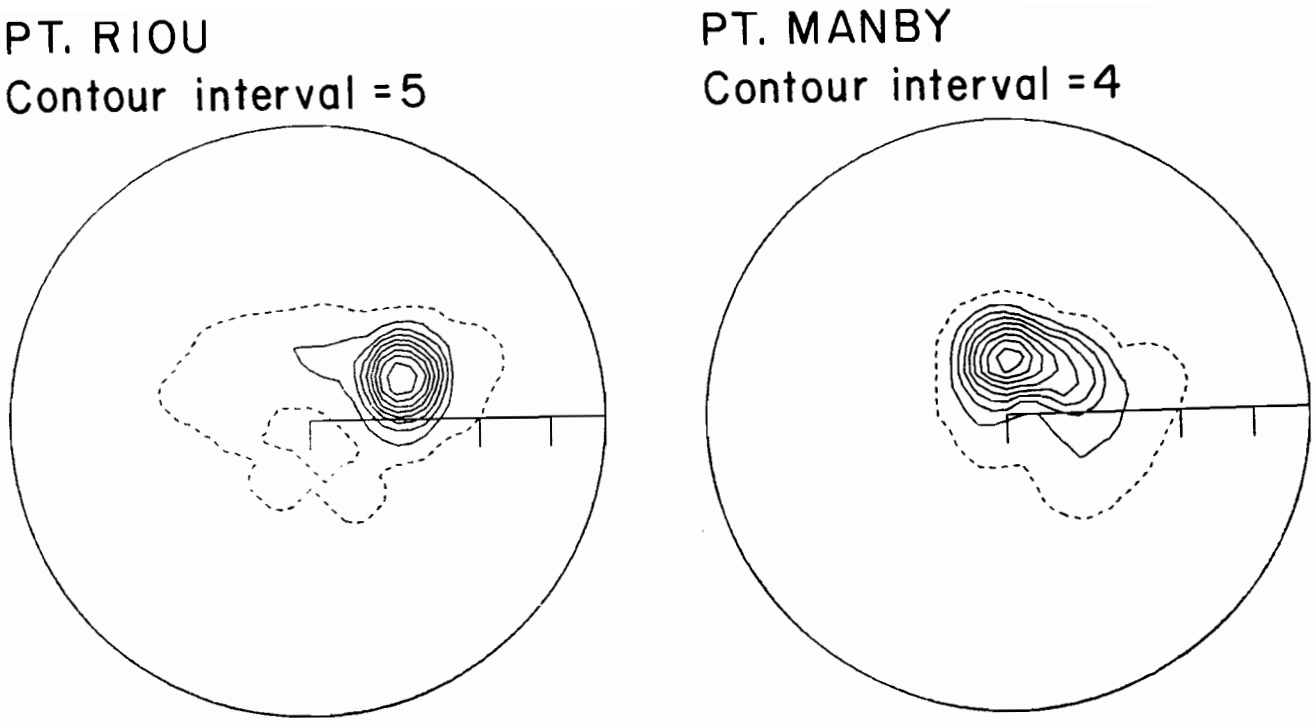

Figure 2.14(a). Wind fabric diagrams for 6 March to 3 April for coastal stations at Pt. Riu and Pt. Manby.

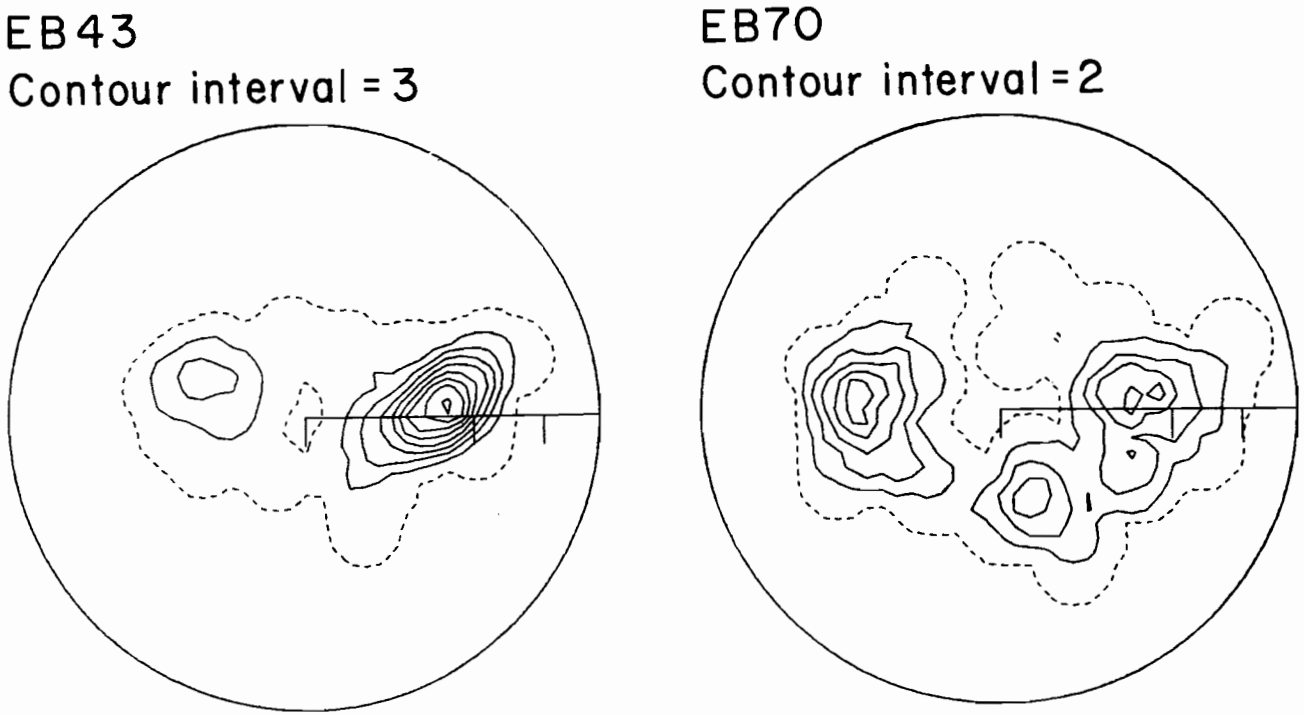

Figure 2.14(b). Wind fabric diagrams for 6 March to 3 April for buoys EB43 and EB70.

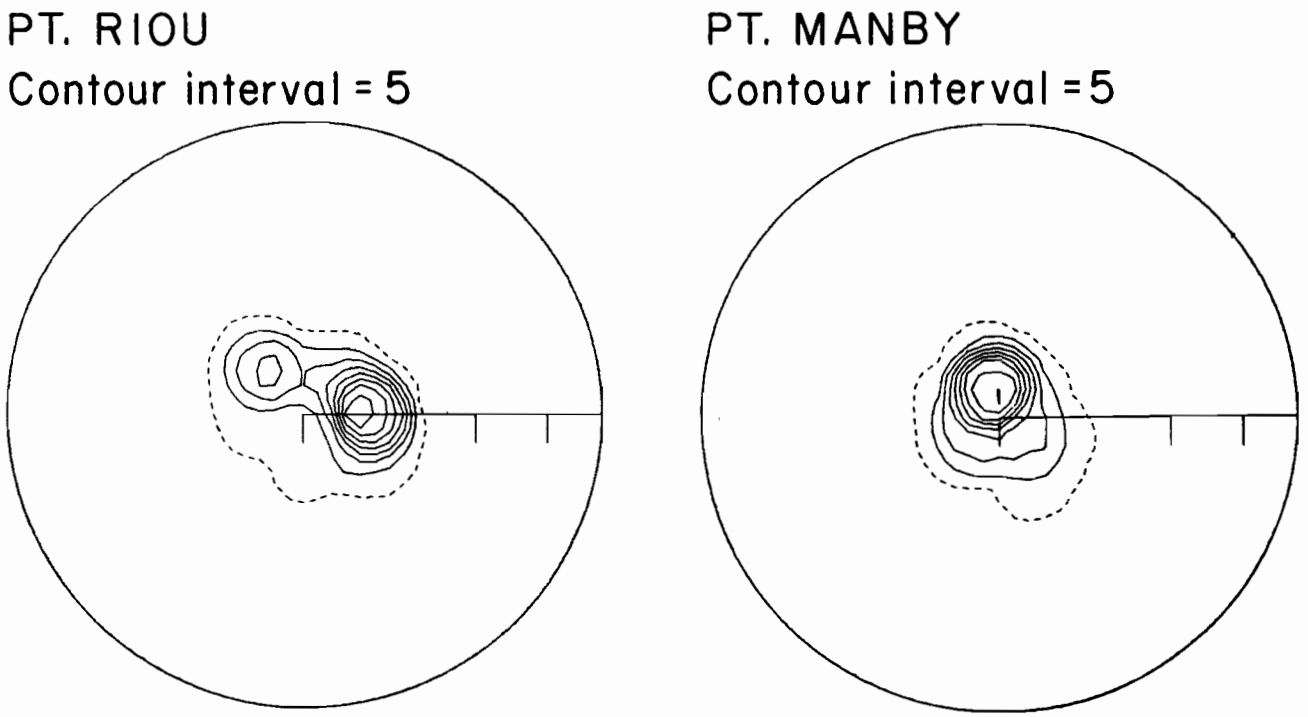

Figure 2.15(a). Wind fabric diagrams for 6 May to 1 June, 1977 for coastal stations at Pt. Riu and Pt. Manby.

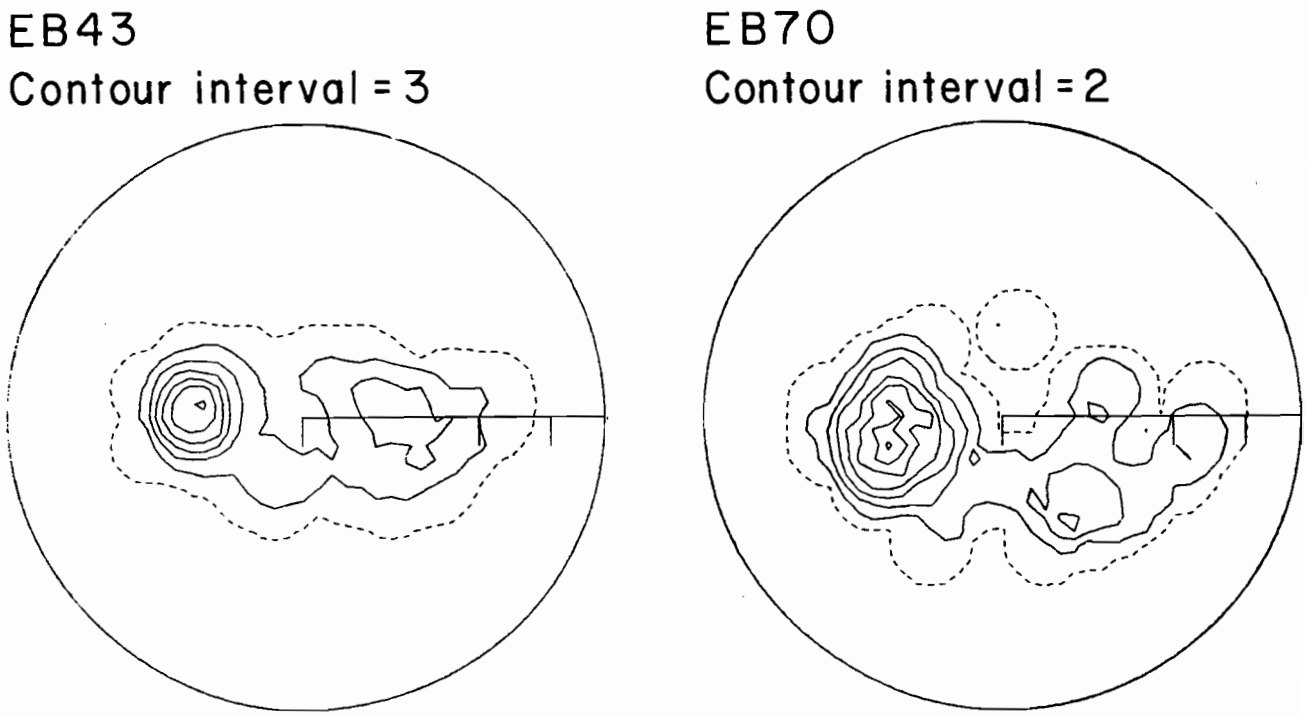

Figure 2.15(b). Wind fabric diagrams for 6 May to 1 June, 1977 for buoys EB43 and EB70.

well-correlated directions. In general, the correlation of wind directions to FNWC steadily deteriorated as the coastline was approached which is evident from the fabric diagrams. However, when data from EB70 is compared with EB43 (Fig. 2.16), an interesting feature is observed. While buoy winds favored an east-west direction, a cluster of points in the upper left-hand corner of the plot indicates occurrences of wind reversal; when EB43 recorded easterly winds, EB70 measured westerlies. The density of the cluster in Figure 2.16 suggests that this was not a rare wintertime occurrence, and the symbol code shows that it happened for a variety of wind speeds, though not with strong winds.

An examination of the original measurements revealed that while both EB70 and EB43 switched directions in a matter of hours, EB43 tended to persist with an easterly flow after EB70 had reversed. The suddenness of wind switching, the greater variation on such small scales, and the poor agreement with FNWC data suggest frontal structure within the mesoscale. During our aircraft study,. discussed below, a small frontal discontinuity which showed such a wind reversal was detected. An offshore katabatic tongue, such as that observed from shipboard measurements, would contribute to the reversals. We note they generally occur in late afternoon with sharp transitions to easterly flow (see Fig. 2.25).

A series of measurements taken from oceanographic ships provided further information on the coastal wind fields. During a cruise aboard the NOAA ship *Oceanographer* on 3 February 1975, a set of radiosondes was released on a trackline orthogonal to the coast. Figure 2.17 summarizes the meteorological observations made by the ship at the time of balloon ascents 6 through 11. The synoptic scale pressure pattern was dominated by an inland high cell that caused the geostrophic wind to be northerly, resulting in offshore advection of the continental air mass. The weather was generally clear with light northerly winds. (See Putnins' weather type H, Fig. 2.8.) EB33 showed cold north winds at this time which confirmed that the flow extended offshore for some distance.

Katabatic drainage winds appear to enhance the weak, offshore flow as shown by measured winds and temperatures at stations 6 and 7 (Fig. 2.17). The flow down the glacier extends 20-30 km offshore where a rather sudden change in direction and temperature occurs. A comparison of near-simultaneous radiosonde profiles from the NWS station at Yakutat and from station 8, 33 km offshore, shows that a strong ground-based inversion at Yakutat was mixed offshore to an altitude of about 500 m. The low-level potential temperature and humidity decreased sharply as the radiosonde broke through the inversion into the dry atmosphere above the mixed layer.

A similar situation existed on 9 March 1976, but the synoptic pressure field was less ambiguous. Surface data were taken and vertical profiles were computed for 35 stations; however, data from only one line of nine stations will be considered here. Observations were made at those nine stations during nearly stationary synoptic conditions (Fig 2.18). Again, a clear progression in surface air temperature was evident along the line of stations.

Wind vectors and temperatures measured by EB33 indicate the air mass was modified by eastward passage over the Gulf of Alaska. However, measurements at Yakutat indicated an offshore flow of cold air.

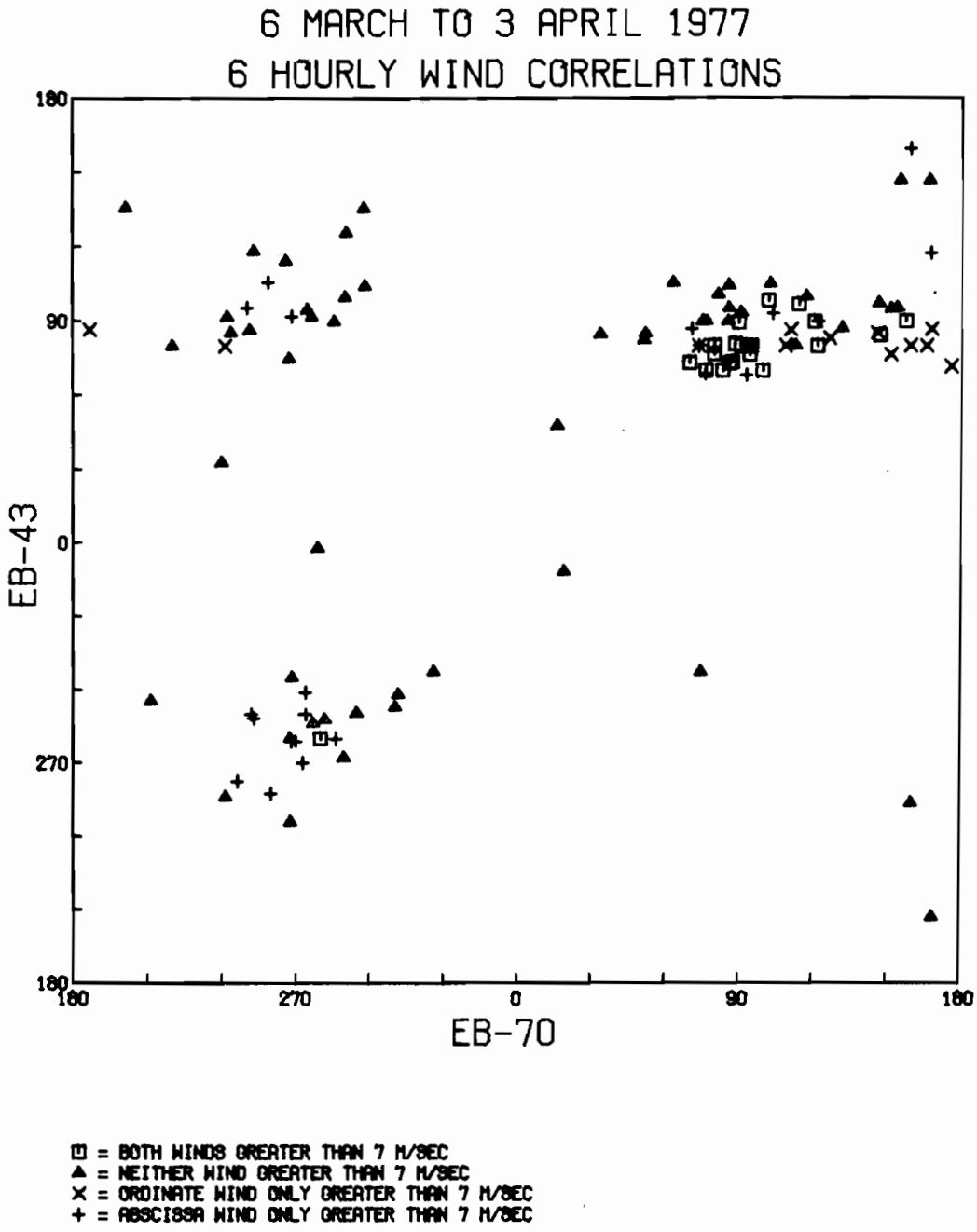

Figure 2.16(a). Correlation plot of wind direction comparing winds at EB43 and EB70 for the period of 6 March to 3 April, 1977.

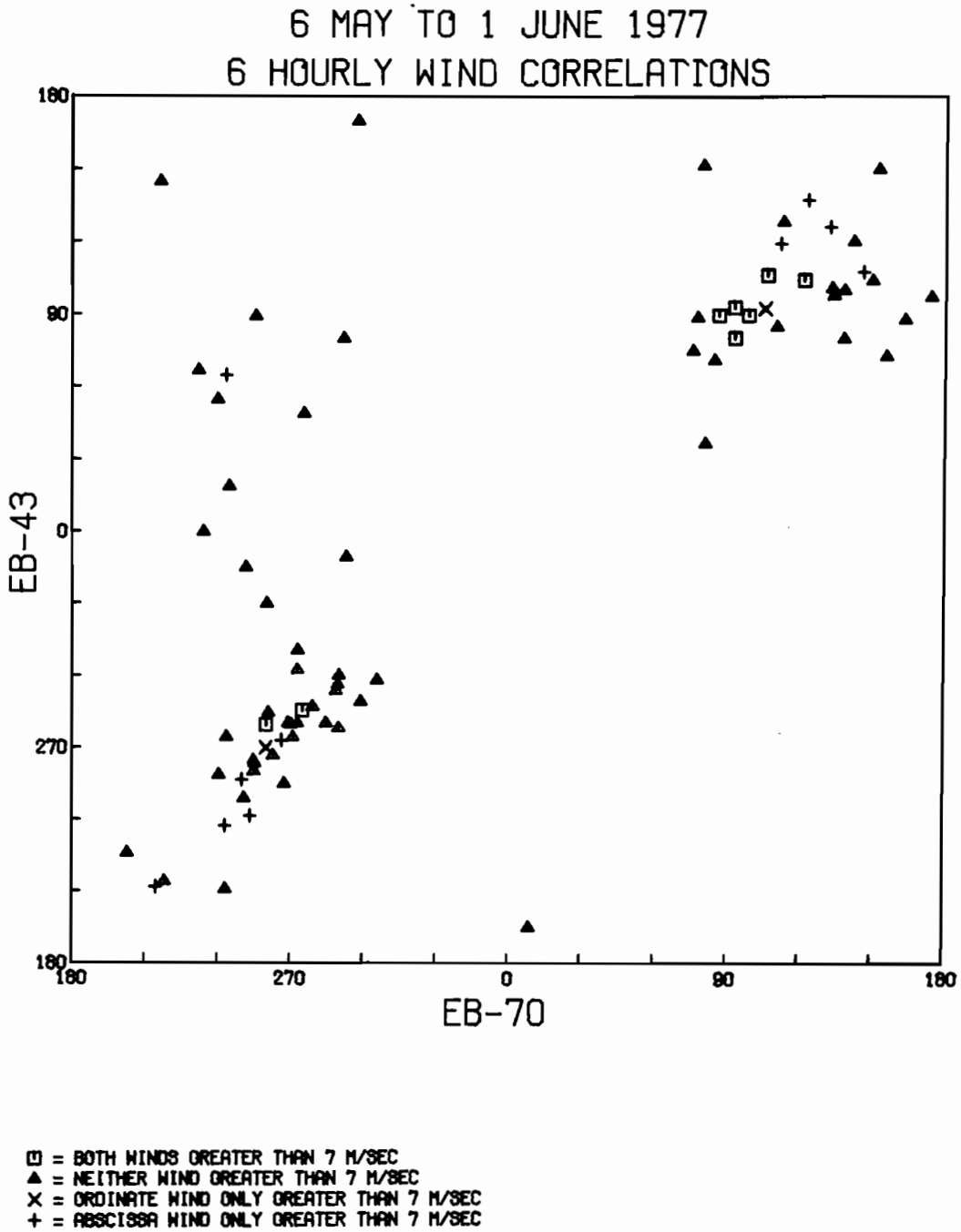

Figure 2.16(b). Same as 2.16(a) for the period 6 May to 1 June, 1977.

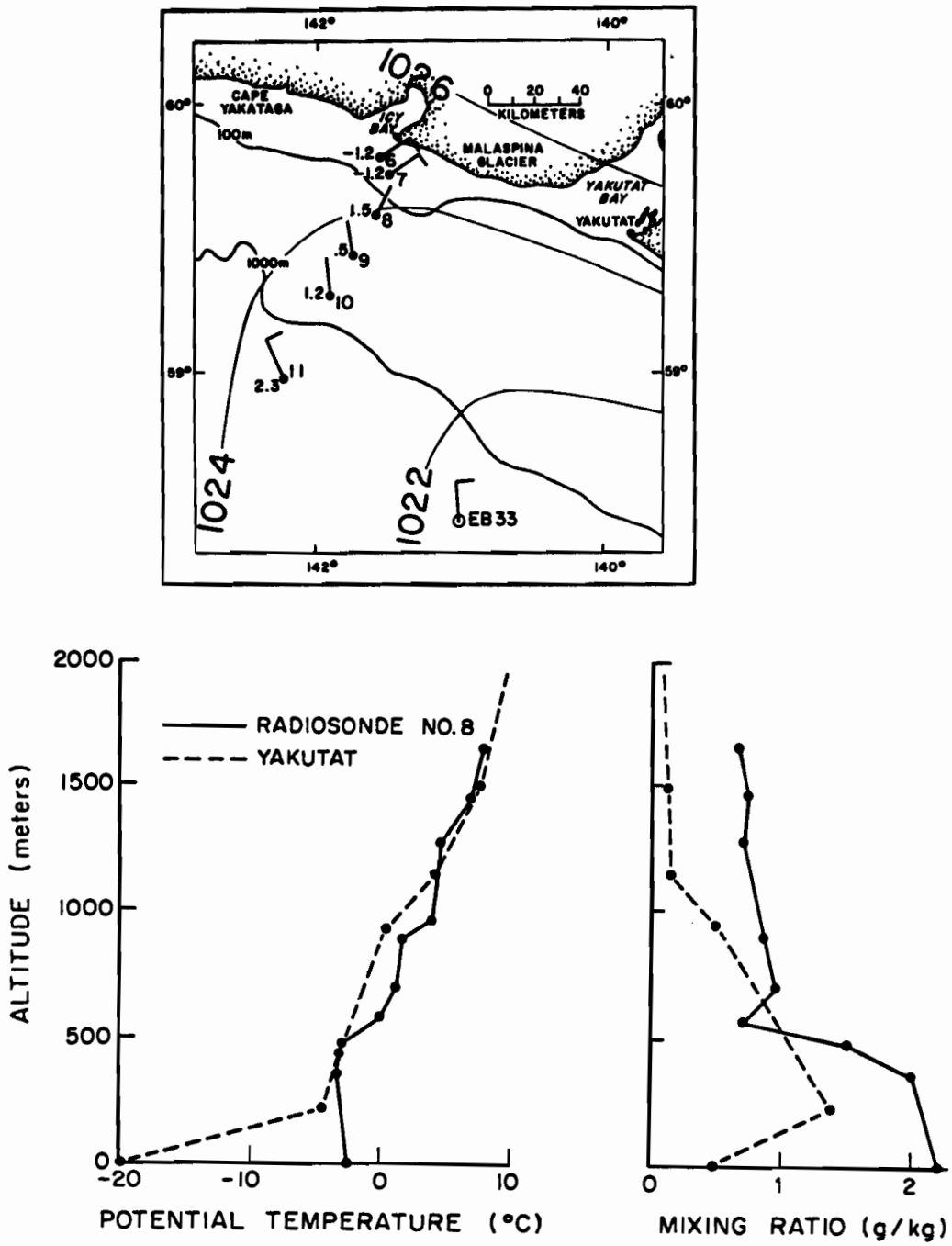

Figure 2.17. Observations of wind and temperature for the 3 February 1975 trackline. The vertical profiles of potential temperature and mixing ratio at station 8 agree well with the Yakutat profile which occured at the same time.

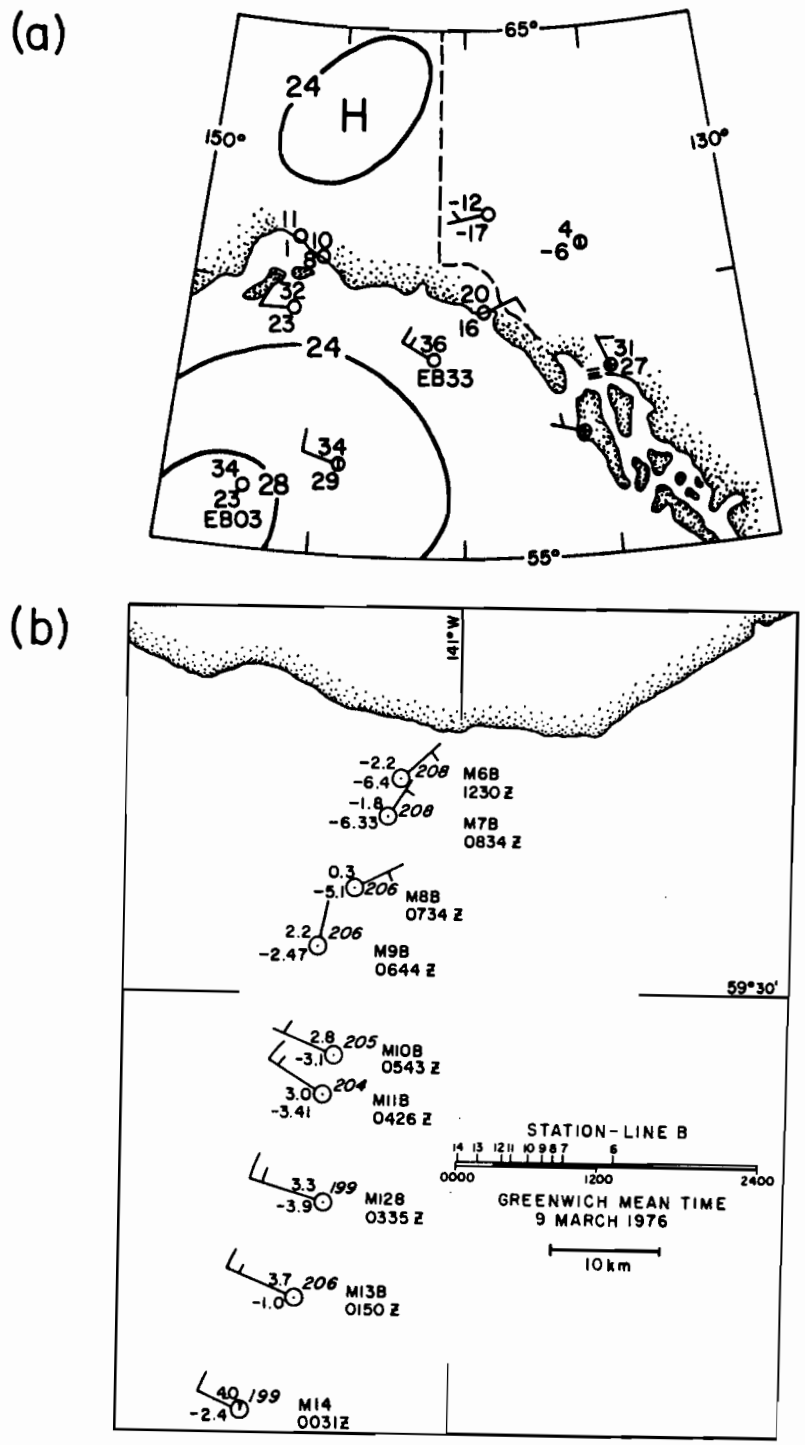

Figure 2.18 (a) Weather map for the Gulf of Alaska-1200 GMT, 9 March 1976. Temperature and dewpoint are in ^{0}F. (b) Surface observations for the 9 March 1976 trackline. Open circles indicate clear skies; temperature (^{0}C), coded pressure (mb), and dewpoint temperature (^{0}C) are shown in clockwise order beginning from a point roughly NW on the symbol.

Again, a thin katabatic flow offshore was rapidly modified by sensible heat transfer from the warm ocean. At about 24 km offshore, the wind arrows (Fig. 2.18) made an abrupt direction change from directly offshore to near-geostrophic. A potential temperature cross section (Fig. 2.19), developed from radiosonde profiles, shows many interesting characteristics of the offshore modification. Katabatic flow was evident as a tongue of cold air extending offshore. The overriding mixed-layer height extended to about 800 m height at 10 km from the coast and about 1400 m at 60 km. The flow of the upper air was approximately into the page, but temperature and inversion height increased offshore. This is partially explained by Figure 2.18; since the flow direction was oblique to the western coast, air farther offshore had been over water for a longer time. Also evident in the cross section was a cold-air core located at 1000 m, about 30 km offshore. Careful examination of the data could not uncover instrumental errors, but there are no firm explanations for this core.

Figure 2.19(b) is a cross section of mixing ratio, contours of which are labeled in g/kg. A weak humidity maximum was evident in the mixed layer. The structure of mixing ratio in a supposedly mixed layer is a result of downward entrainment of dry air aloft (Mahrt, 1976). The height of the maximum varied from 240 m at the coast to 580 m at 60 km offshore.

A kytoon profile (Fig 2.20) showed a convective mixed layer extending from the surface to about 30 m. This was capped by a very stable katabatic layer to about 250 m. At this point a transition from the low-level northerly katabatic flow to the westerly synoptic-scale wind field occurred. There was some indication of overshoot, typical of nocturnal jet phenomena observed above stable ground-based inversions (Blackadar, 1957). The profile is similar to profiles measured by Sholtz and Brouchaert (1978) where the air is stable well above the height of direction transition.

The wind speed reached a near-zero minimum above 240 m, and the stability began decreasing toward the neutral value observed aloft. Somewhere between stations 9 and 10 (between 20 and 28 km offshore) the surface convective layer must penetrate the katabatic "lid", designated by the level of abrupt direction change, thereby allowing a downward mix of westerly momentum with resulting surface westerlies.

In February and March 1977 the *Queen Air* (see Section 2.1) made flights over the glacier and coastal waters. During much of the experimental period the 500 mb flow was dominated by the same large-amplitude wave that caused unseasonal winter weather over most of the United States and Canada. Low pressure in the Bering Sea and a ridge along western North America cooperated to drive most storms onshore in Southeast Alaska. The 500 mb geostrophic winds were, on the average, southwesterlies. At the surface, low-pressure systems in the Gulf of Alaska and north central Pacific persistently moved northeastward into the Bering Sea causing south or southeast geostrophic flow in the Yakutat area. Such conditions are not conducive to the development of cold drainage winds from the north. Post-frontal weather usually consisted of continued southerly winds bringing stratocumulus clouds and light rain or snow showers. Taken all together, these conditions gave Yakutat an unseasonably warm and wet year with very little snowfall. Of seven flights, one in particular is interesting in the context of this dissertation; 1900-2300Z, 25 February 1977.

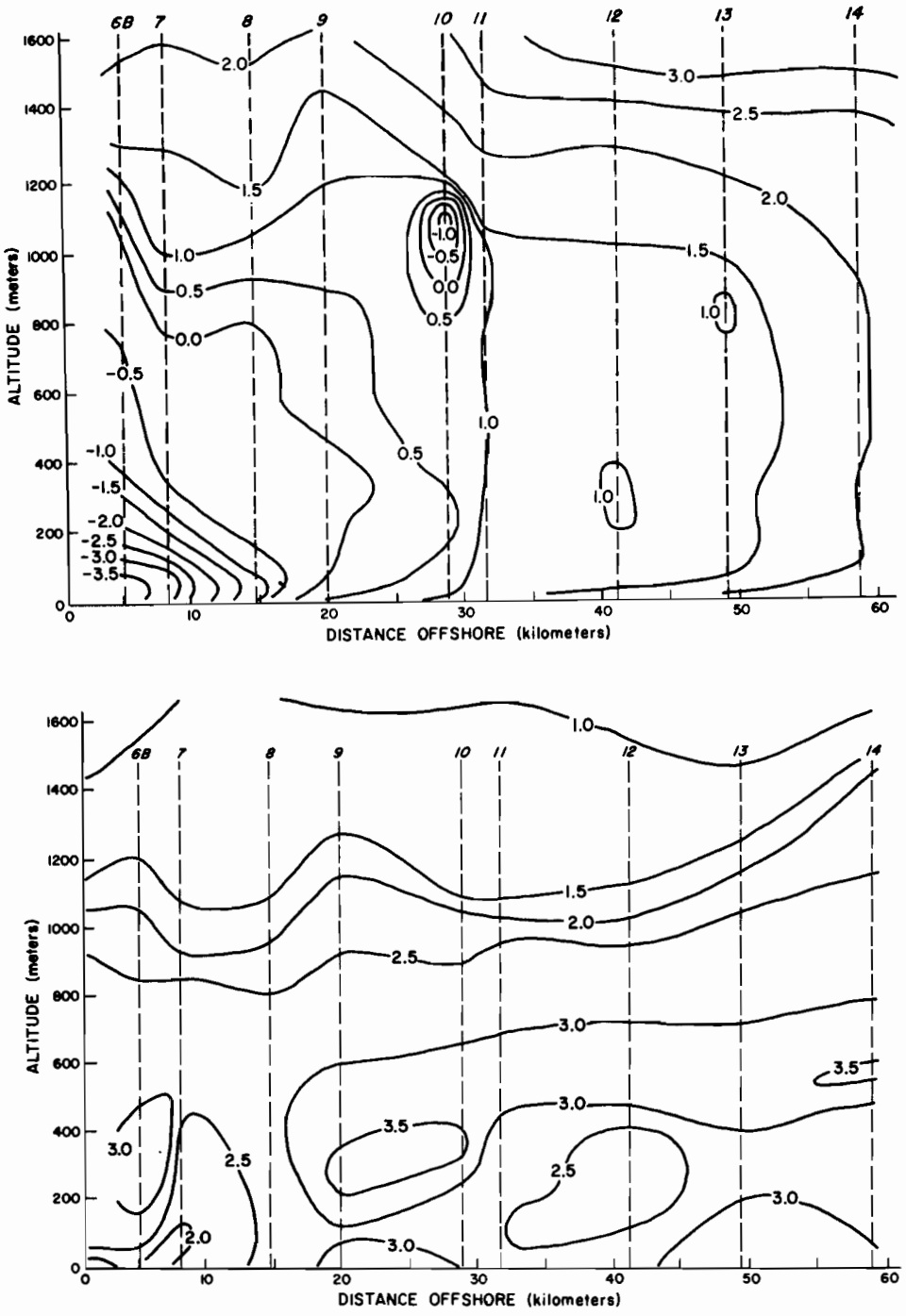

Figure 2.19. Contour plot of (a) potential temperature and (b) mixing ratio as a function of distance offshore. Of note are the katabatic cold wedge and cold core at 1000 m.

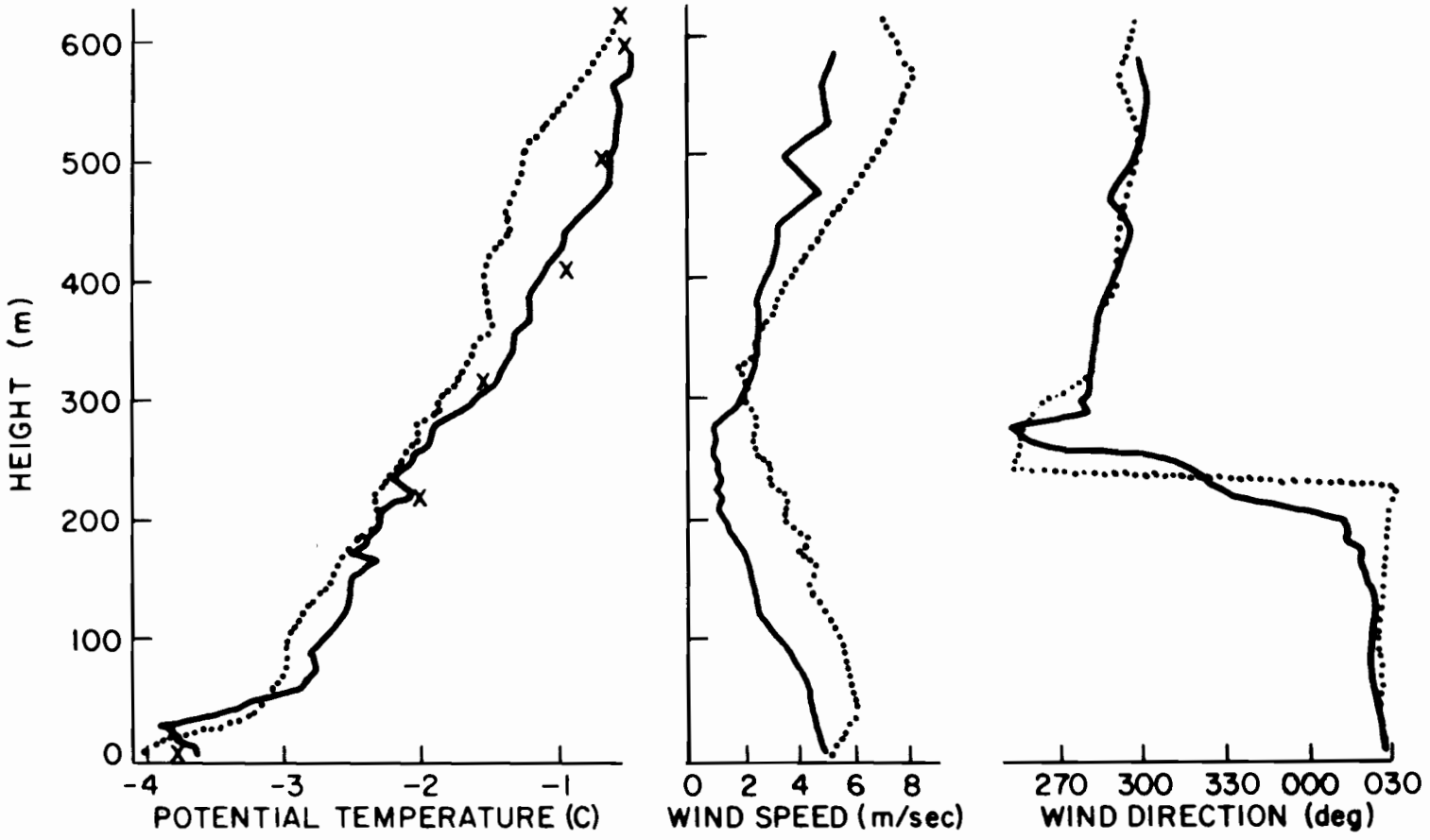

Figure 2.20. Profiles of temperature and winds from radiosonde (x), tethered balloon ascent (solid line), and descent (dotted line) taken at station 6, about 6 km offshore. Wind direction indicates a sharp transition at 250 m. There is evidence of a shallow mixed layer at 30 m.

The 12Z, 25 February, 500 mb and 18Z, surface analyses are shown in Figure 2.21. At 500 mb, a trough south of Yakutat on the previous day turned into a small, closed, low-pressure center. In the study region the pressure gradient aloft was very weak, as evidenced by Yakutat's meager 10 m/s winds from the southwest. At the surface a front from the previous day had dissipated with mostly clear air moving in behind. A low-pressure center to the southeast produced a bunching of the isobars at the coast with relaxed gradient offshore. The pattern here is similar to the 3 February 1975 case described earlier. The geostrophic pattern created a well-defined, low-speed, longshore surface flow in the study area with weaker flow occurring seaward.

The sky was clear except for some small cumulus about 25 km offshore of the Malaspina Glacier. A satellite photo (Fig. 2.22) showed these clouds clearly as a very thin fingerlike protrusion spiralling into a small broken cumulus center about 100 km south-southwest of Icy Bay. This barely discernible cloudy patch is shown below to be associated with dramatic changes in the wind field on this day.

Aircraft soundings from way points 8 (the glacier, solid line) and 9 (offshore, dotted line) and the Yakutat rawinsonde sounding (dashed line) are compared in Figure 2.23. Low-level longshore flow at Yakutat is evident from the surface wind direction and moist surface mixing-ratio profile. Although the Yakutat potential temperature profile does not indicate a marine mixed layer near the surface as one would expect under longshore flow conditions, this is probably a reflection of the crudity of the rawinsonde analysis. The aircraft potential temperature sounding over the Malaspina Glacier clearly shows a mixed layer extending from about 325 m to 550 m. The wind in this layer is light and easterly. Below, the wind is stronger, drier, and blows out of the interior indicating substantial low-level drainage. Sixty kilometers offshore the aircraft sounding shows a homogeneous boundary layer, well mixed to 500 m.

The startling difference in the wind directions observed in the two aircraft soundings is better seen in the 30-m altitude offshore distributions (Fig. 2.24). Within an interval of a few hundred meters the wind speed dropped from 5 m/s to 1 m/s. The temperature and humidity likewise showed sudden changes. The wind direction was much slower to respond, taking 10 to 15 km to shift to a nearly steady direction. Aboard the aircraft, we noted an increase in the turbulence intensity as this front was penetrated. Subsequent passes at higher levels showed that this event persisted at least throughout the mixed layer, although the changes through this front weakened with height.

Inshore from the front, the flow situation presented here is remarkably similar to the case of 9 March 1976. Katabatic flow undercuts neutrally stratified marine air having a longshore wind component. As the drainage winds pass the coast, a super-adiabatic layer develops at the air-sea interface as a result of the vigorous heat flux; this layer grows in height with offshore fetch until it completely penetrates the katabatic tongue approximately 30 km offshore. Beyond there is little resistance to mixing over a whole lower layer to 500 m, and properties of the upper portion of this layer are mixed downward to the surface.

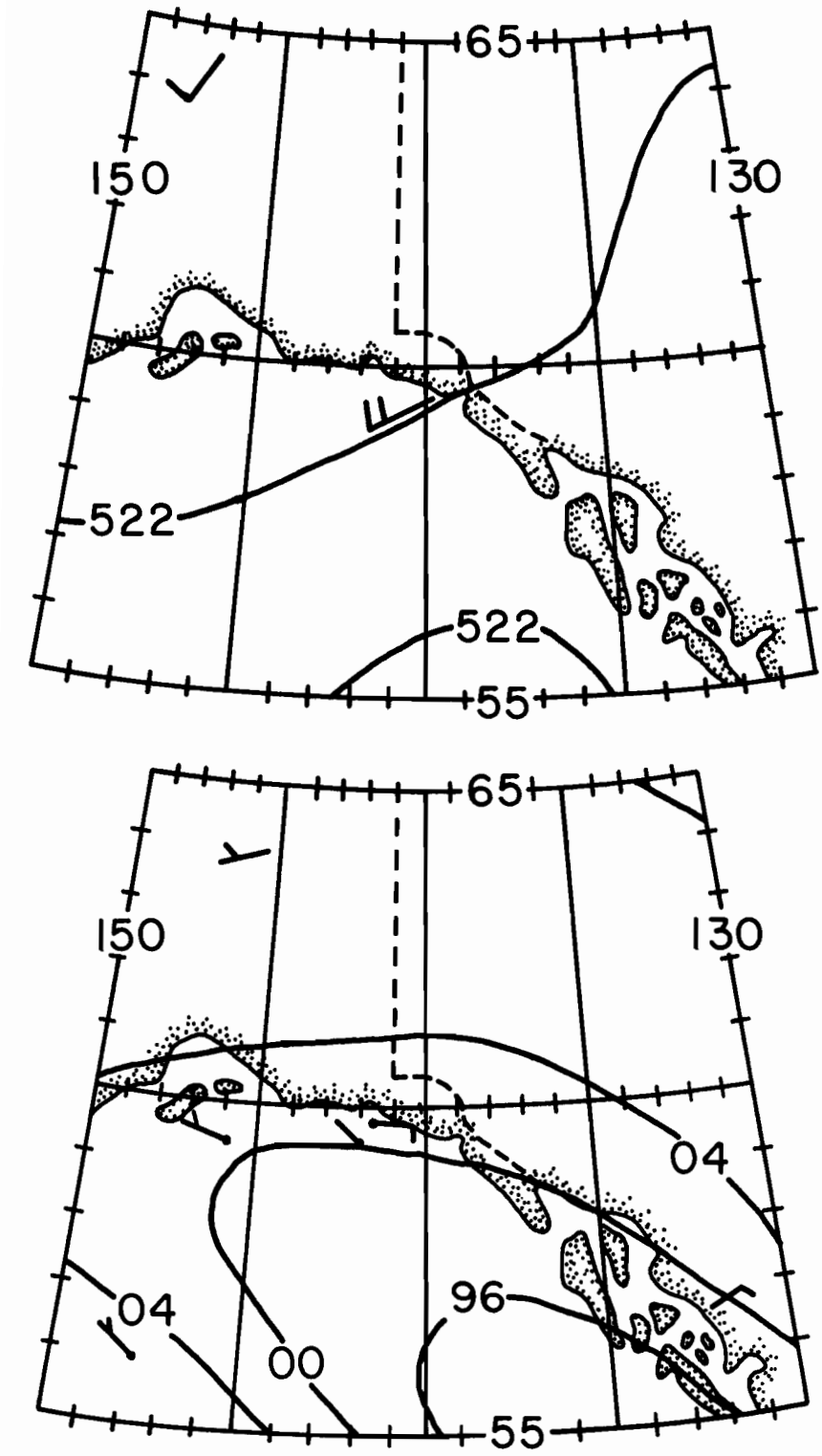

Figure 2.21. Weather during the Queen Air flight on 25 February 1977. The upper map is the 12Z, 500 mb chart and the lower map is the 18Z, surface chart. Observed winds are plotted on the maps.

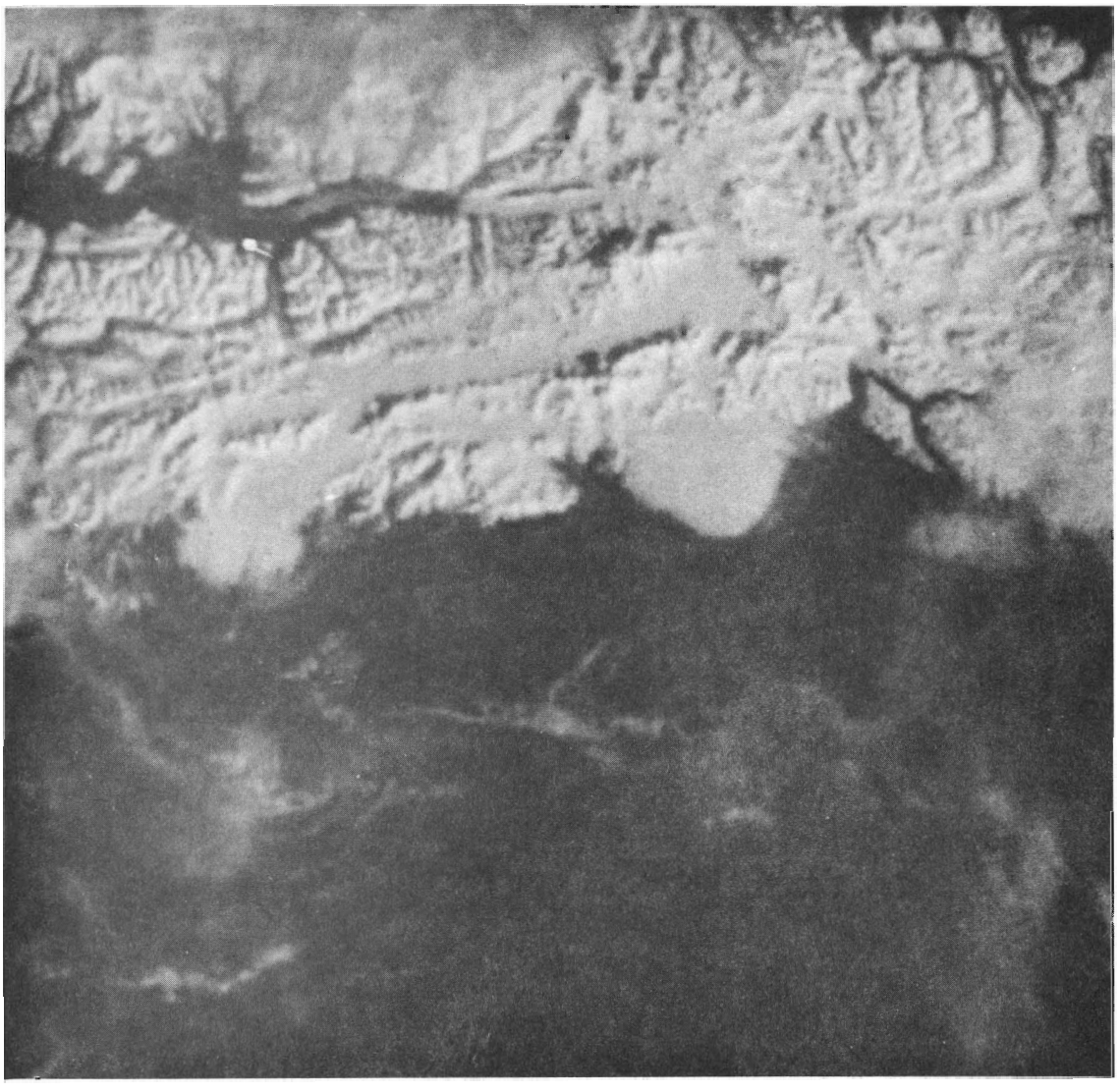

Figure 2.22. Satellite photo of the Gulf of Alaska on 25 February 1977.

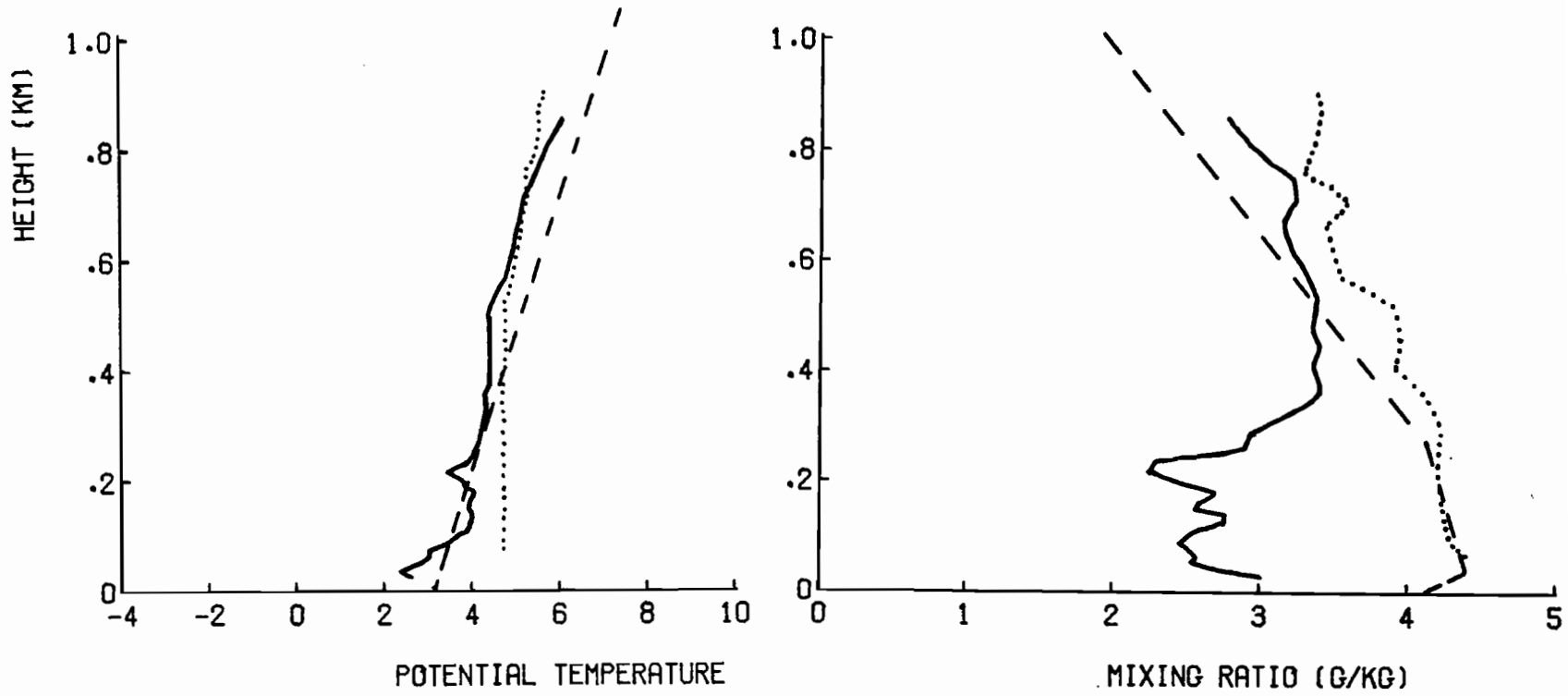

Figure 2.23(a). Vertical profiles of potential temperature and mixing ratio taken by the Queen Air during the flight. The solid line is at the inshore point, in the vicinity of stations 6-8. The dotted line is offshore, station9. The dashed line is a sounding taken at Yakutat NWS at the same time.

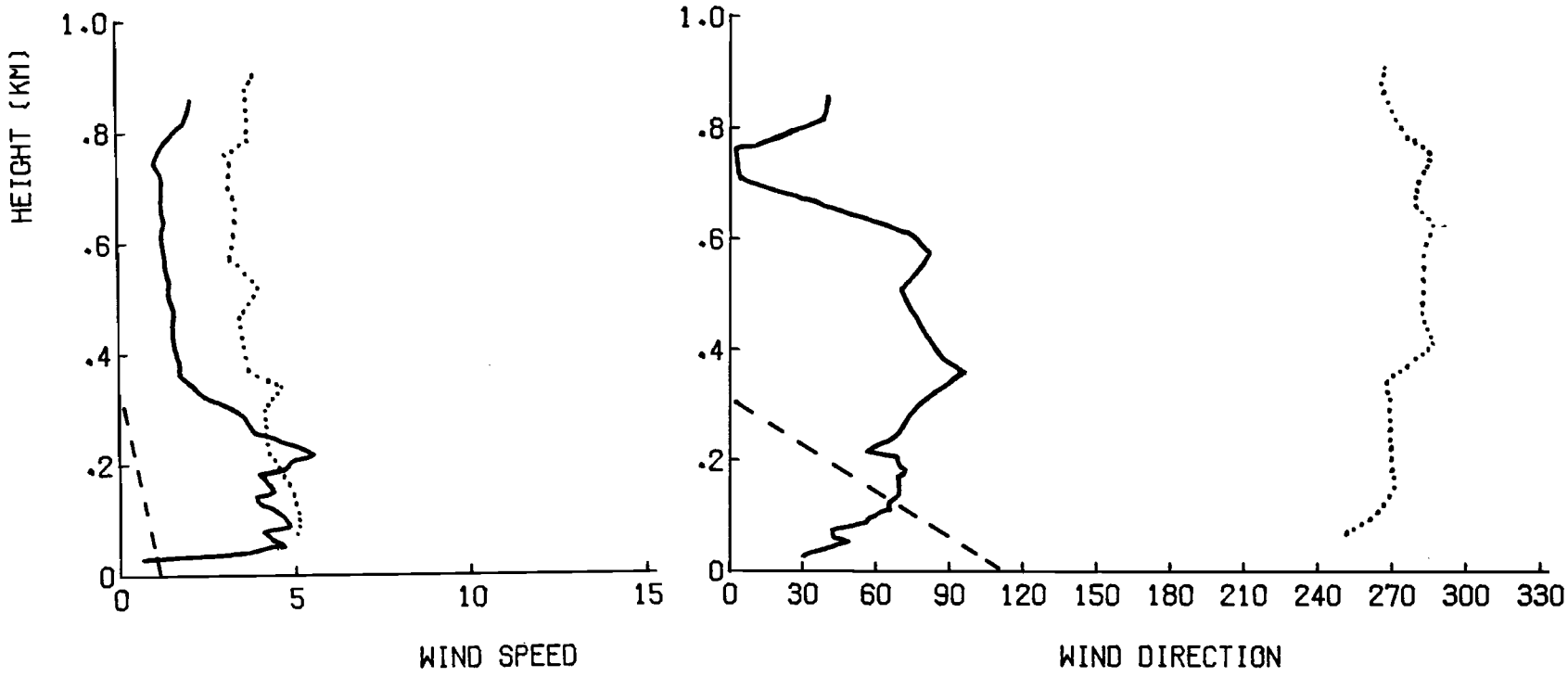

Figure 2.23(b). Same as 2.23(a) for wind speed and wind direction.

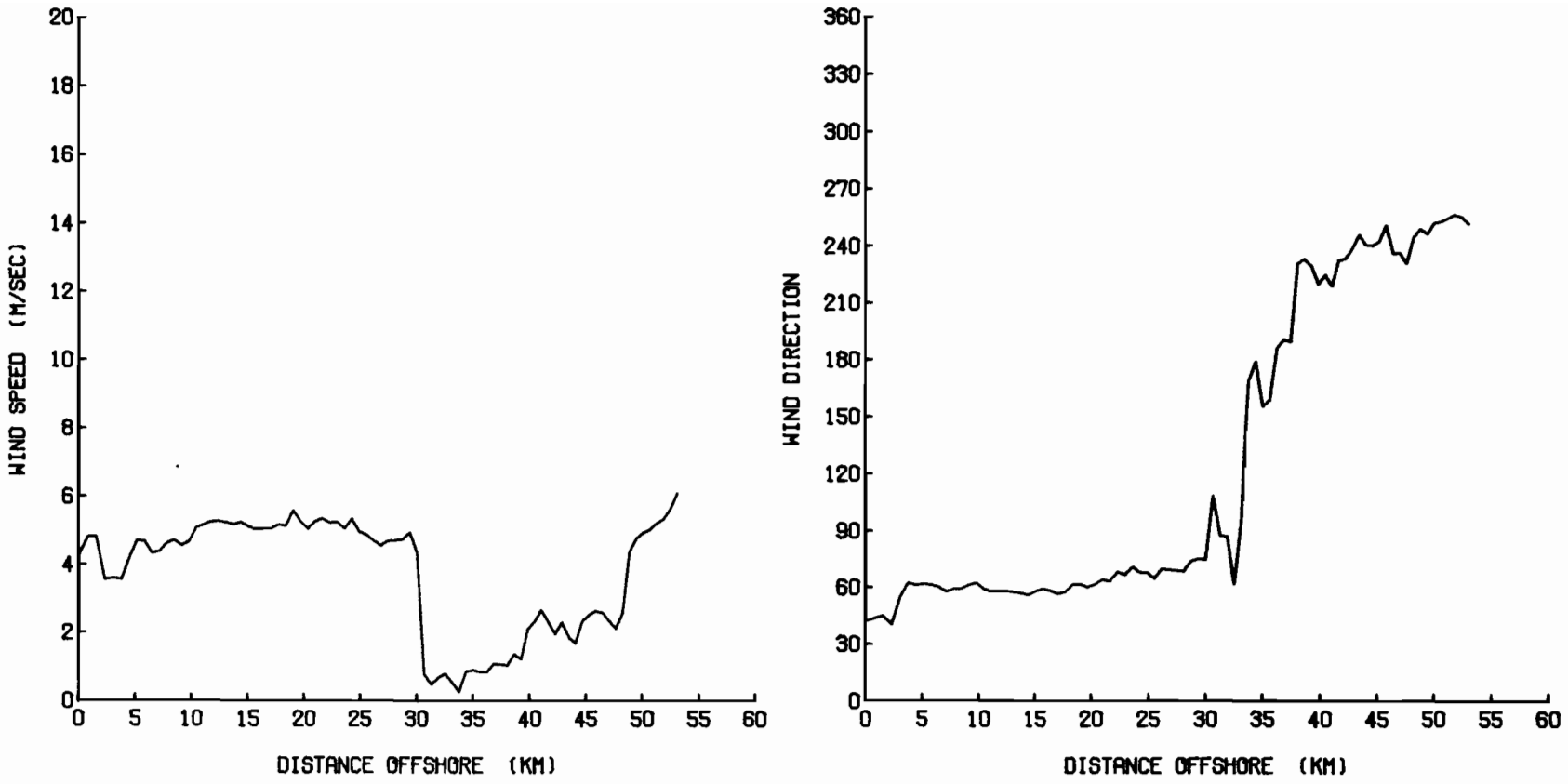

Figure 2.24a. Distribution of wind speed and direction along the offshore trackline. Data are instantaneous from an altitude of 30 m.

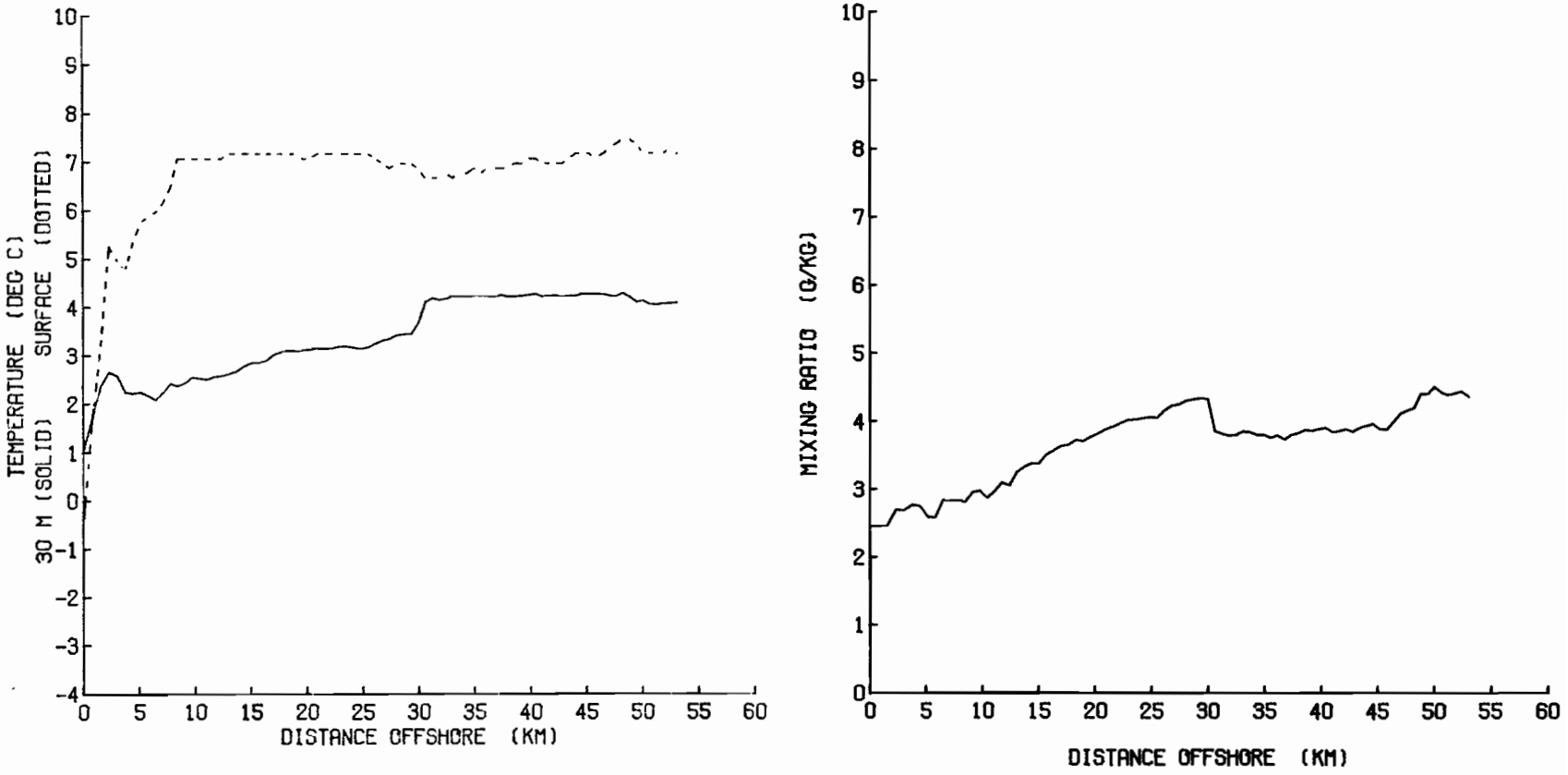

Figure 2.24b. Distribution of temperature and mixing ratio along the offshore trackline. Data are instantaneous from an altitude of 30m. The dashed line is sea surface temperature as inferred from infra-red radiation.

Still unexplained is the mechanism for the change in the offshore wind direction from 100° (the expected geostrophic direction) near the coast to 270° forty kilometers offshore. The event is apparently related to the mesoscale patch of cloudiness mentioned above. The NWS surface analysis for 06Z on February 26 shows a small low-pressure cell in this region. While such mesoscale features may not be commonplace, they are certainly not exceptional in these coastal regions.

At 60 m altitude, 11 km horizontally averaged spatial distributions of wind speed and direction, air temperature, mixing ratio, and sea surface temperature are shown in Figure 2.25. Several features noted in all aircraft flights are apparent here. First an increase in wind speed occurs with westward passage across the mouth of Yakutat Bay to the south end of the Malaspina Glacier. This coastal jet blowing along the flanks of the glacier may occur from confluence of air blowing across the mouth of the Bay with air blowing out its western shore. Air at the Icy Bay side of the glacier is warmer and drier. Sea surface temperature exhibits a pronounced long-shore gradient from Yakutat Bay to Icy Bay. This cooling amounts to about .02°C/km.

3. CONCLUSION

In conclusion, the St. Elias Mountain range, a rather abrupt coastal demarcation, has a noticeable effect on the movement and development of cyclonic disturbances in the Gulf of Alaska. There is an observed retardation in movement of the isobaric surfaces on the coastal side of the cell, and the mesoscale wind field in the vicinity of the Malaspina Glacier shows local orographic control sufficient to invalidate synoptic analyses. Near-coastal wind measurements show a pronounced east-west (the general orientation of the mountain range) bimodality but tend toward a synoptic fit about 100 km offshore.

In the case of a low pressure offshore, drainage of cold continental air from the interior produces intense katabatic fall winds which enhance the background katabatic drainage winds (Fig. 3.1(a)). Such a situation is common on this coast and explains a predominance of cold easterlies as observed at the NDBO buoys, especially EB43 closer to shore.

Otherwise, the weak katabatic drainage (Fig. 3.1(b)) underrides the neutral marine airmass. As it flows offshore, an internal mixed layer grows until it warms to the temperature of the overriding mixed layer and a sudden shift in the winds accompanies the intermixing of the layers.

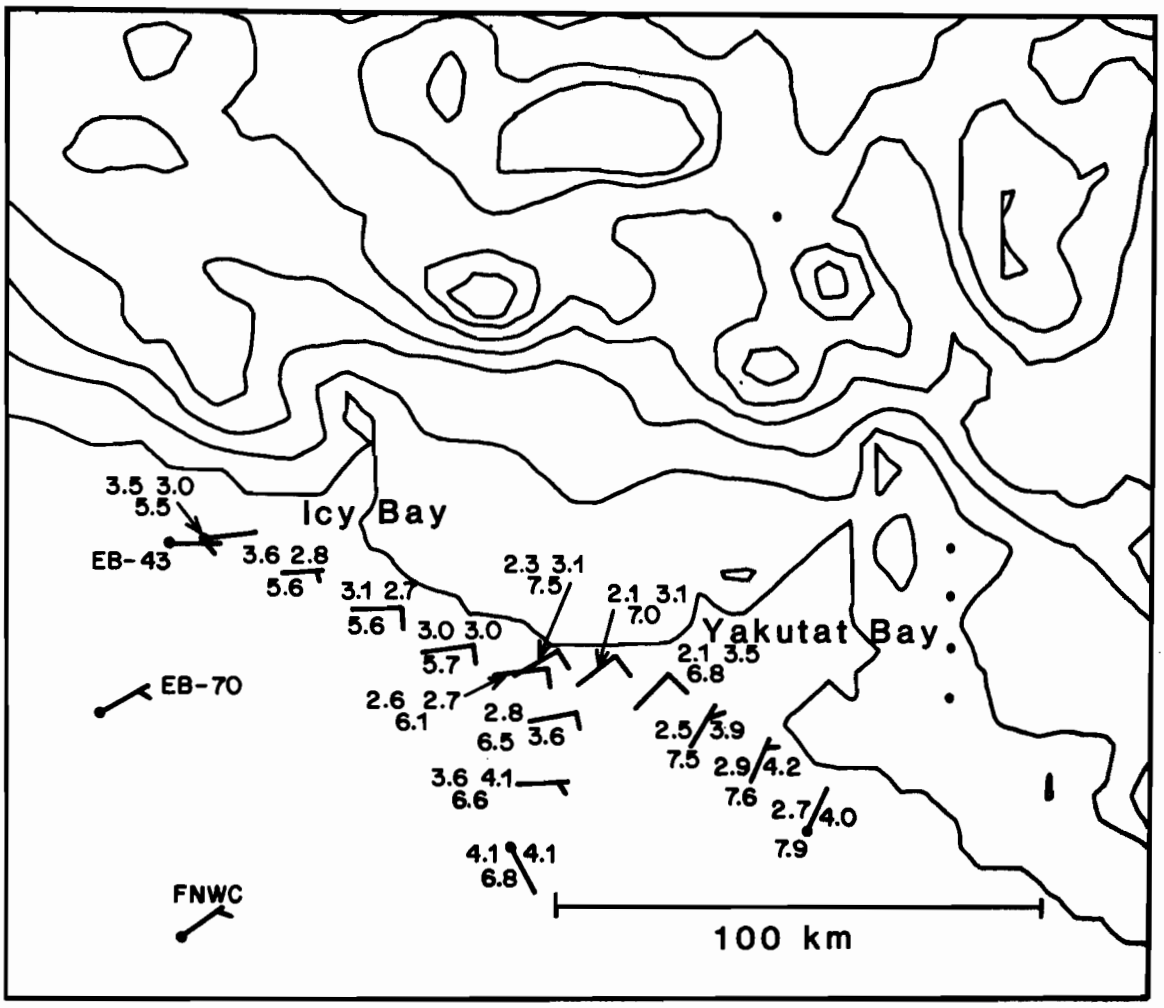

Figure 2.25. Winds measured during the Queen Air flight. The data are from an altitude of 60 m and are horizontal averages over about 11 km.

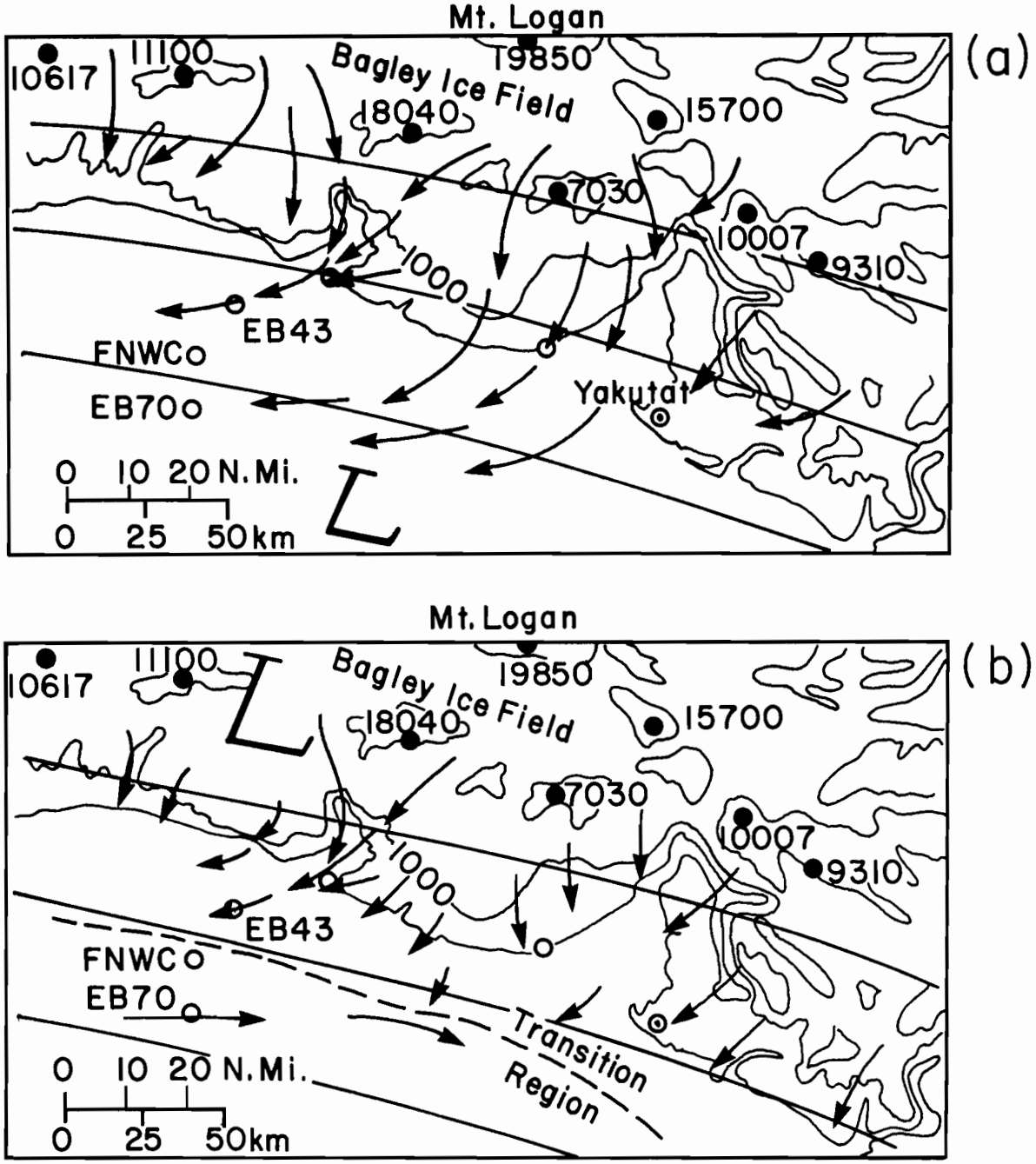

Figure 3.1. Example of flow conditions at the Malaspina Glacier which could lead to the observed winds and temperature anomolies at the data buoys.

4. REFERENCES

Bakun, A., 1973: Coastal Upwelling Indices, West Coast of North America, 1946-71, NOAA Tech. Rept. NMFS SSRF-671, 103 pp.

Ball, F.K., 1960a: Winds on the Ice Slopes of Antarctica. Pro. of the Symp. on Antarctic Meteorology, J.W. Arrowsmith Ltd., Bristol, Great Britain, pp. 9-16.

Bilelo, M.S., 1974: Air Masses, Fronts and Winter Precipitation in Central Alaska. Cold Regions and Engineering Laboratory Report, 85 pp.

Blackadar, A.K., 1975: Boundary Layer Wind Maxima and Their Significance for the Growth of Nocturnal Inversions. Bull. Amer. Meteor. Soc., 38, pp. 283-290.

Businger, J.A., 1954: Some Aspects of the Influence of the Earth's Surface on the Atmosphere. Med. Verh. Kon. Ned. Meteor. Inst., No. 61, 78 pp.

Businger, J.A., 1972: The Atmospheric Boundary Layer. Remote Sensing of the Troposphere, Chap. 6, U.S. Dept. Commerce, NOAA.

Ching, Jason Kwok Sung, 1974: Determination of the Surface Stress Using the Vorticity Equation and the Mass Budget Results from BOMEX Data. Ph.D. Dissertation, University of Washington, 103 pp.

Davis, B.L. and M.W. Ekern, 1977: Wind Fabric Diagrams and Their Application to Wind Energy Analysis. J. Appl. Meteor., 16, pp. 552-531.

Defant, F., 1960: Local Winds. Compendium of Meteorology, T.F. Malone, Ed., Amer. Meteor. Soc., pp. 665-672.

Godshall, F.A., W.R. Sequin, and P. Sabol, 1976: Analysis of Ship Surface Meteorological Data Obtained During GATE Intercomparison Periods. Center for Experiment Design and Data Analysis Working Document, Environmental Data Service, NOAA, 67 pp.

Huschke, R.E., 1959: Glossary of Meteorology. Am. Meteor. Soc., 638 pp.

Kilday, G.D., 1970: Taku Winds at Juneau, Alaska, NWS Office Memo, Juneau, Alaska, 8 pp.

Lenschow, D.H., 1972: The measurement of Air Velocity and Temperature Using the NCAR Buffalo Aircraft Measuring System. NCAR Technical Notes, NCAR-TN/EDD-74, National Center for Atmospheric Research, Boulder, 39 pp.

Macklin, S.A., R.W. Lindsay, and R.M. Reynolds, 1980: Observations of mesoscale winds in an Orographically-Dominated Estuary: Cook Inlet, Alaska. Second Conference on Coast Meteorology, January 30 - February 1, 1980. American Meteorology Society.

Mahrt, L.F., 1974: Time-Dependent Integrated Planetary Flow. J. Atmos. Sci., 31, pp. 457-464.

Mahrt, L.F., 1976: Mixed Layer Moisture Structure. Mon Weather Rev., 104, pp. 1403-1407.

Putnins, P., 1966: Studies on the Meteorology of Alaska, Environmental Data Services, Silver Springs, MD, 90 pp.

Reynolds, R.M., 1980: On the Dynamics of Coastal Winds. Ph.D. Dissertation, University of Washington, 176 pp.

Scholtz, M.T. and C.J. Brouckaert, 1978: Modeling of Stable Air Flow Over a Complex Region, J. Appl. Meteorl, 17, pp. 1249-1257.

Searby, H.W., 1969: Coastal Weather and Marine Data Summary for the Gulf of Alaska, Cape Spencer Westward to Kodiak Island. ESSA Tech. Memo. EDSTM8, 30 pp.

Yoshino, M.M., 1975: Climate In A Small Area. University of Tokyo Press, 549 pp.